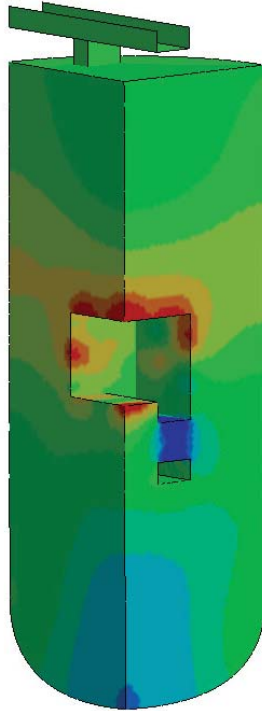




LUND
UNIVERSITY



FLUID-STRUCTURE INTERACTION

Numerical modelling and experimental comparison

JOHAN LINDGREN and HANNES KARLSSON

Structural
Mechanics

Master's Dissertation

DEPARTMENT OF CONSTRUCTION SCIENCES
DIVISION OF STRUCTURAL MECHANICS

ISRN LUTVDG/TVSM--17/5227--SE (1-60) | ISSN 0281-6679

MASTER'S DISSERTATION

FLUID-STRUCTURE INTERACTION

Numerical modelling
and experimental comparison

JOHAN LINDGREN and HANNES KARLSSON

Supervisors: **JAN STENVALL**, MSc, Division of Structural Mechanics, LTH
and **HENRIK ENGSTRÖM**, MSc, Saab Kockums AB.

Examiner: Professor **KENT PERSSON**, Division of Structural Mechanics, LTH.

Copyright © 2017 Division of Structural Mechanics,
Faculty of Engineering LTH, Lund University, Sweden.

Printed by Media-Tryck LU, Lund, Sweden, June 2017 (*PI*).

For information, address:

Division of Structural Mechanics,
Faculty of Engineering LTH, Lund University, Box 118, SE-221 00 Lund, Sweden.

Homepage: www.byggmek.lth.se

Abstract

The purpose of this thesis is to investigate the effects of fluid-structure interaction on a submerged oscillating structure. It is to be determined whether it is possible to model such effects with acoustic fluid elements in LS-DYNA using Mat_Acoustic. Experiments of an oscillating submerged box were performed and the results were used to compare simulations of the same setups. The setups comprised of 4 different oscillating frequencies and the optional addition of a plate inducing more fluid-structure interaction. From the experiments, an analysis of the rate of decay was performed and a two term exponential model was proposed.

The results showed that added mass is consistently underestimated by 15% in the FE-model. Furthermore the plate resulted in an increase of added mass for the experiment and the FE-model.

Additionally, convergence studies regarding the required fluid volume to assume infinite depth and fluid mesh sizing were performed and the results were presented as dimensionless quantities. General guidelines on how to use Mat_Acoustic and maintain stability were presented. Structure shell elements proved to be particularly difficult to model in terms of stability.

Sammanfattning

Målet med examensarbetet är att undersöka påverkan av fluid-struktur interaktionen för en svängande kropp nedsänkt i vatten. Vidare är det undersökt huruvida det går att modellera denna typ av fenomen med akustiska element i LS-DYNA med Mat_Acoustic. Experiment med en svängande låda utfördes för att kunna jämföras med simuleringar av samma uppsättning. Experimenten innefattade fyra olika svängningsfrekvenser och en bottenplatta kunde dessutom läggas till för att öka fluid-struktur interaktionen. För experimentdatan utfördes en analys av dämpningen och en exponentialfunktion med två termer föreslogs för att beskriva den.

Resultaten visade att den virtuella massan konsekvent underskattades med 15% i FE-modellen för det givna fallet. Utöver det visades det även att tillägget av bottenplattan resulterade i en ökning av virtuell massa för både experimentet och FE-modellen.

Konvergensstudier angående den volym som krävs för att antagandet oändligt vattendjup skall vara giltig genomfördes även. Konvergensstudier genomfördes även för storleken av fludelementen.

Generella riktlinjer för hur Mat_Acoustic bör användas för att bibehålla stabilitet presenteras även. Strukturer modellerade med skalelement visade sig vara speciellt svårmodellerade med hänsyn till stabilitet.

Acknowledgements

We would like to thank Kockums for this great opportunity to perform an interesting thesis in the field of submarine development. To work in a professional test center has been educational for us as well as being a joyous experience. We would like to express our gratitude to the staff at the test center for their help and advice. Shout out to Micke for his banter.

We would especially like to thank Henrik Gunnarsson for his patience and for his efforts in helping us. Without his help we would never have been able to conduct the experiments.

Our supervisors Jan Stenvall and Henrik Engström have been of great importance to us. They have helped us in our planning, given us advice and guidance in times of trouble.

Henrik Engström has with his experience in modelling been a tremendous resource to us. We have learned a lot from his advice which has increased our knowledge in modelling. This will be of help to us in the future.

Jan Stenvall has been a great source of motivation to us. His door has always been open and to him there is no such thing as a stupid question. Jan has with his experience in submarine development provided us with great amounts of relevant information and interesting conversations. His knowledge of military history is truly remarkable.

We would also like to express our gratitude toward our examiner Kent Persson whose input helped improve the quality of this paper.

Contents

1	Introduction	1
1.1	Background	1
1.2	Objectives and Aim	1
2	Theory	3
2.1	Mass-Spring System	3
2.1.1	Damped Mass-Spring System	3
2.2	Finite Element Method	3
2.2.1	Structural Domain	4
2.2.2	Eulerian vs Lagrangian vs Arbitrary Lagrangian-Eulerian	5
2.3	Numerical Simulation	5
2.3.1	The Central Difference Method	5
2.4	Butterworth Filters	5
2.5	Fluid-Structure Interaction	6
2.5.1	Mat_Acoustic	6
2.5.2	Displacement Potential	6
2.5.3	Acoustic Wave Equation	7
2.6	Concept of Added Mass	7
2.6.1	Natural Frequency in Fluid	7
2.6.2	Analytical Solution for Added Mass	8
3	Experiments	9
3.1	Experimental Setup	9
3.1.1	The Design of The Box	11
3.1.2	Measuring Devices	12
3.2	Experimental Procedure	13
3.2.1	Sources of Error and Assumptions	14
3.3	Experimental Results in Air	15
3.4	Experimental Results in Water	15
3.4.1	Displacement	16
3.4.2	Acceleration	16
3.4.3	Pressure	17
3.4.4	Strain	17
3.5	Added Mass	18
3.6	Summation of Results	19
3.7	Validation of Results	19
3.7.1	Influence of Water Level	19
3.7.2	Influence of Amplitude	21
3.7.3	Verification of Acceleration and Displacement	21
3.7.4	Decay	23
3.7.5	Decay in air	25
3.8	Discussion	27
4	Modelling	29
4.1	Model Setup in LS-Prepost	29
4.2	Implemented Keywords	31
4.2.1	Box and Frame	31
4.2.2	Acoustic Volume	31
4.2.3	Discrete Elements	31
4.2.4	Hourglassing and Control Keywords	31
4.3	Sources of Error in Simulations	32
4.4	Modelling Results	32
4.4.1	Displacement	32
4.4.2	Velocity	33
4.4.3	Acceleration	34
4.4.4	Pressure	34
4.5	Frequency Domain and Filtering	36
4.5.1	Velocity	36

4.5.2	Acceleration	37
4.5.3	Pressure	38
4.6	Added Mass Simulations	39
4.7	Convergence studies	40
4.7.1	Fluid Mesh Size for Solid Elements	40
4.7.2	Fluid Mesh Size for Shell Elements	41
4.7.3	Fluid Volume	44
4.8	Discussion	45
5	Comparison between Experiment and Simulation	47
5.1	Displacement	47
5.2	Acceleration	47
5.3	Pressure	48
5.4	Summation of Results	48
5.5	Discussion	50
6	Conclusion	51
7	Recommendations for Use of Mat_Acoustic	53
8	Future work	55
A	Keywords	59
A.1	Box and Frame	59
A.2	Fluid Volume	59
A.3	Springs	60
A.4	Hourglassing and Control Keywords	60
B	Measuring devices	61

1 Introduction

1.1 Background

Equipment mounted on the hull on the outside of a submarine may be subjected to shock loading from different types of explosions. An underwater explosion will produce several shock waves and will make the equipment exhibit a dynamic response. To accurately model the oscillations of the equipment, it is important to capture the fluid-structure interaction between the equipment and the surrounding fluid. Such models already exist and are based on the finite element method. It is also common practice to use analytical methods. The Swedish shipyard Kockums is interested in assessing acoustic elements in fluid modelling. This is of interest as the acoustic elements in question only utilize one degree of freedom thus being very computationally efficient.

However, a model using acoustic elements has not been sufficiently validated with respect to experimental data. A better understanding of the limitations when using acoustic elements will help improve the design of mounted equipment and may be used in the development of the next generation of submarines.

1.2 Objectives and Aim

The aim of this thesis is to assess how well the material model `Mat_Acoustic` in LS-DYNA captures the fluid-structure interaction of a submerged oscillating structure. Added mass in particular is used as a quantification of the fluid-structure interaction. In order to assess `Mat_Acoustic`, experiments are to be conducted so that the results can be compared to a similar FE-model. The FE-model will be created in LS-Prepost and the fluid is to be modelled using `Mat_Acoustic`. The model will then be solved using LS-DYNA R8.1.0 with an explicit solver. An analysis regarding the limitations and accuracy of the acoustic model will be presented as well as convergence studies on mesh sizing and fluid volume sizing.

2 Theory

2.1 Mass-Spring System

To get a basic understanding of the experimental setup, the equations for a one degree of freedom mass-spring system with no damping are here presented. Hooke's law describes the force needed to extend or compress a spring

$$F = -ku \quad (2.1)$$

F is the force needed to change the length of a spring with the stiffness k a distance u . Newton's second law yields the equation of motion

$$m\ddot{u} + ku = 0 \quad (2.2)$$

By assuming a harmonic solution $u = A \sin(\omega_n t + \phi)$ and differentiating twice with respect to time, eq. (2.2) can be written as

$$kA \sin(\omega_n t + \phi) = m\omega_n^2 A \sin(\omega_n t + \phi) \quad (2.3)$$

If trivial solutions are ignored

$$\omega_n = \sqrt{\frac{k}{m}} \quad (2.4)$$

The natural frequency may thus be written as

$$f_n = \frac{1}{2\pi} \sqrt{\frac{k}{m}} \quad (2.5)$$

2.1.1 Damped Mass-Spring System

Only some key equations are presented here and the reader is referred to a book in engineering mechanics for a more detailed explanation (e.g. [13]).

The damped angular frequency can be expressed as

$$\omega_d = \omega_n \sqrt{1 - \zeta^2} \quad (2.6)$$

where ω_n is the undamped frequency and ζ is the damping ratio. The function that represents the exponential damping of the motion can be expressed in the following way

$$y(t) = C e^{-\zeta \omega_n t} \quad (2.7)$$

The damping ratio ζ can be determined experimentally by obtaining two successive amplitudes x_1 and x_2 [13, p. 590]. If eq. (2.7) holds then

$$\frac{x_1}{x_2} = \frac{C e^{-\zeta \omega_n t}}{C e^{-\zeta \omega_n (t+T_d)}} = e^{\zeta \omega_n T_d} \quad (2.8)$$

where T_d is the damped period. Defining the logarithmic decrement as

$$\delta = \ln \frac{x_1}{x_2} \quad (2.9)$$

and inserting into eq. (2.8) yields

$$\delta = \zeta \omega_n T_d \quad (2.10)$$

which can be arranged to

$$\zeta = \frac{\delta}{\sqrt{(2\pi)^2 + \delta^2}} \quad (2.11)$$

using equation eq. (2.6) and that $T_d = \frac{2\pi}{\omega_d}$. Eq. (2.11) can be used to calculate the damping ratio.

2.2 Finite Element Method

The finite element method is a numerical method used to solve differential equations in an approximate manner. The differential equation describing a physical phenomena is said to hold over an entire region [16, ch. 1]. The region where the differential equation is valid is divided into finite elements. By dividing the region into smaller elements, approximations regarding the variation of a certain variable in a specific element become simpler compared to approximations over the entire region. The simpler approximation of each element enables an approximation for the entire region. A system of equations can be assembled and solved which yields a solution for the entire region.

2.2.1 Structural Domain

To give a brief introduction of the theory behind the FEM, the FE-formulation for the structural domain is presented as it is quite simple compared to the fluid domain. The notation used in this derivation is based on [3]. The equations of motions for the structure can be expressed as

$$\tilde{\nabla}^T \boldsymbol{\sigma}_s + \mathbf{b}_s = \rho_s \frac{\partial^2 \mathbf{u}_s}{\partial t^2} \quad (2.12)$$

where the displacement \mathbf{u}_s , the stress $\boldsymbol{\sigma}_s$, the strain $\boldsymbol{\epsilon}_s$ and the body force \mathbf{b}_s can be written as

$$\mathbf{u}_s = \begin{bmatrix} u_1^s \\ u_2^s \\ u_3^s \end{bmatrix} \quad \mathbf{b}_s = \begin{bmatrix} b_1^s \\ b_2^s \\ b_3^s \end{bmatrix} \quad \boldsymbol{\sigma}_s = \begin{bmatrix} \sigma_{11}^s \\ \sigma_{22}^s \\ \sigma_{33}^s \\ \sigma_{12}^s \\ \sigma_{13}^s \\ \sigma_{23}^s \end{bmatrix} \quad \boldsymbol{\epsilon}_s = \begin{bmatrix} \epsilon_{11}^s \\ \epsilon_{22}^s \\ \epsilon_{33}^s \\ 2\epsilon_{12}^s \\ 2\epsilon_{13}^s \\ 2\epsilon_{23}^s \end{bmatrix} \quad (2.13)$$

The density of the structure is denoted ρ_s and

$$\tilde{\nabla}^T = \begin{bmatrix} \frac{\partial}{\partial x_1} & 0 & 0 & \frac{\partial}{\partial x_2} & \frac{\partial}{\partial x_3} & 0 \\ 0 & \frac{\partial}{\partial x_2} & 0 & \frac{\partial}{\partial x_1} & 0 & \frac{\partial}{\partial x_3} \\ 0 & 0 & \frac{\partial}{\partial x_3} & 0 & \frac{\partial}{\partial x_1} & \frac{\partial}{\partial x_2} \end{bmatrix} \quad (2.14)$$

The constitutive and kinetic equations can be written as

$$\boldsymbol{\epsilon}_s = \tilde{\nabla} \mathbf{u}_s \quad \text{and} \quad \boldsymbol{\sigma}_s = \mathbf{D}_s \boldsymbol{\epsilon}_s \quad (2.15)$$

where \mathbf{D}_s is the constitutive matrix. To derive the weak form, eq. (2.12) is multiplied by a weight function \mathbf{v}_s and integrated over the structural domain.

$$\int_{\Omega_s} \mathbf{v}_s^T (\tilde{\nabla}^T \boldsymbol{\sigma}_s - \rho_s \frac{\partial^2 \mathbf{u}_s}{\partial t^2} + \mathbf{b}_s) dV = 0 \quad (2.16)$$

Using the Green-Gauss theorem yields the weak form of the differential equation:

$$\int_{\Omega_s} \mathbf{v}_s^T \rho_s \frac{\partial^2 \mathbf{u}_s}{\partial t^2} dV + \int_{\Omega_s} (\tilde{\nabla} \mathbf{v}_s)^T \boldsymbol{\sigma}_s dV - \int_{\partial \Omega_s} (\mathbf{v}_s)^T \mathbf{t}_s dS - \int_{\Omega_s} \mathbf{v}_s^T \mathbf{b}_s dV = 0 \quad (2.17)$$

where the traction, $\mathbf{t}_s = \mathbf{S}_s \mathbf{n}_s$, \mathbf{n} is the normal vector pointing outwards from the boundary of the structural domain and

$$\mathbf{S}_s = \begin{bmatrix} \epsilon_{11} & \epsilon_{12} & \epsilon_{13} \\ \epsilon_{12} & \epsilon_{22} & \epsilon_{23} \\ \epsilon_{13} & \epsilon_{23} & \epsilon_{33} \end{bmatrix} \quad (2.18)$$

By introducing element shape functions N_s , the nodal displacements of the structure can be expressed as

$$\mathbf{u}_s = \mathbf{N}_s \mathbf{a}_s \quad (2.19)$$

Furthermore, the weight function can be written as

$$\mathbf{v}_s = \mathbf{N}_s \mathbf{c} \quad (2.20)$$

where \mathbf{c} is an arbitrary parameter. Combining eq. (2.19) and (2.15) yields

$$\boldsymbol{\epsilon}_s = \tilde{\nabla} \mathbf{N}_s \mathbf{a}_s = \mathbf{B}_s \mathbf{a}_s \quad (2.21)$$

Inserting eq. (2.19), (2.15), (2.20) and (2.21) into eq. (2.17) gives the finite element formulation for the structure

$$\mathbf{M}_s \ddot{\mathbf{a}}_s + \mathbf{K}_s \mathbf{a}_s = \mathbf{f}_f + \mathbf{f}_b \quad (2.22)$$

where

$$\mathbf{M}_s = \int_{\Omega_s} \mathbf{N}_s^T \rho_s \mathbf{N}_s dV \quad \mathbf{K}_s = \int_{\Omega_s} \mathbf{B}_s^T \mathbf{D}_s \mathbf{B}_s dV \quad (2.23)$$

and

$$\mathbf{f}_f = \int_{\partial \Omega_s} \mathbf{N}_s^T \mathbf{t}_s dS \quad \mathbf{f}_b = \int_{\Omega_s} \mathbf{N}_s^T \mathbf{b}_s dV \quad (2.24)$$

The differential equation from eq. (2.12) has now been transformed into a set of integrals that can be solved numerically for every element. The Finite element formulation holds for every element and can be combined into a large set of equation for the entire domain.

2.2.2 Eulerian vs Lagrangian vs Arbitrary Lagrangian-Eulerian

There are different ways of formulating the frame of reference in a finite element program. Here, a brief overview of the three different approaches is presented.

A Lagrangian mesh moves and deforms with the material. It is mainly used in structural analysis and the method handles time dependant constitutive relations well. Inasmuch as the mesh moves with the material, tracking of free surfaces and interfaces is easy [6, Ch. 14]. The approach may however cause inaccuracies if the material experiences large deformations so that the elements become distorted [14].

An Eulerian mesh is fixed in space and the behaviour is thus calculated with respect to the original position. This type of formulation is commonly used in fluid dynamics. It models large deformations more accurately, but at the expense of the resolution of the flow [6, Ch. 14].

An arbitrary Lagrangian-Eulerian mesh combines the Lagrangian and Eulerian method in an effort to minimize the drawbacks of the two methods while maintaining their respective strengths [6, Ch. 14]. An Eulerian formulation is used in `Mat_acoustic`

2.3 Numerical Simulation

Dynamic simulations in LS-DYNA can be performed using both an implicit and an explicit solver. An implicit solver requires the stiffness matrix to be inverted at least once per time step which is an expensive operation for large models. Therefore an implicit solver is unsuitable when small time steps are needed such as for transients. Inverting the stiffness matrix is not needed for an explicit solver thus it is better suited for shorter simulations where small time steps are needed [12]. The major drawback is that the explicit solver does not enforce equilibrium thus possibly making the solution nonphysical.

2.3.1 The Central Difference Method

LS-DYNA uses the central difference method, which is an explicit solver, to solve the equation of motion. In this section, a brief derivation of the method is presented [9]. The semi-discrete equations of motion at time n are given by

$$\mathbf{M}\mathbf{a}_n = \mathbf{P}_n - \mathbf{F}_n \quad (2.25)$$

where \mathbf{M} is the mass matrix, \mathbf{P}_n is external and body forces, and \mathbf{F}_n is the stress divergence vector. Note that the hourglass resistance is not included here as it does not provide any further insight in how the equations of motions are solved. Also note that this is a more general form of the equation of motion in (4.1). In order to solve for the next timestep, the acceleration is calculated based on (2.25).

$$\mathbf{a}_n = \mathbf{M}^{-1}(\mathbf{P}_n - \mathbf{F}_n) \quad (2.26)$$

The acceleration can be used to calculate the velocity half a time step later.

$$\mathbf{v}_{n+\frac{1}{2}} = \mathbf{v}_{n-\frac{1}{2}} + \mathbf{a}_n \Delta t_n \quad (2.27)$$

This in turn can be used to calculate the new displacement

$$\mathbf{u}_{n+1} = \mathbf{u}_n + \mathbf{v}_{n+\frac{1}{2}} \Delta t_{n+\frac{1}{2}} \quad (2.28)$$

where

$$\Delta t_{n+\frac{1}{2}} = \frac{(\Delta t_n + \Delta t_{n+1})}{2} \quad (2.29)$$

The geometry is updated by adding the displacements to the initial configuration

$$\mathbf{x}_{n+1} = \mathbf{x}_0 + \mathbf{u}_{n+1} \quad (2.30)$$

2.4 Butterworth Filters

In the analysis of the results, filters were used to process the data. Lowpass filters were used to filter the data obtained in the simulations and highpass filters were used in the integration of the acceleration.

Butterworth filters are specified by its cutoff frequency and its filter order. The filter order determines the sharpness of the transition from the stopband to the passband at the cutoff frequency [15]. A pre-written first-order filter in MATLAB was used to filter the data.

2.5 Fluid-Structure Interaction

To model fluid structure interaction in LS-DYNA the fluid is modelled as transient acoustic elements by use of Mat_Acoustic.

2.5.1 Mat_Acoustic

Mat_Acoustic is a material model in LS-DYNA designed for low-pressure acoustic shock wave propagation and can only be used with the acoustic pressure element formulation [8]. The elements are linear and Eulerian [5]. Mat_Acoustic uses displacement potential to solve the acoustic wave equation (sec. 2.5.3) and therefore only requires one degree of freedom per node [11]. This makes Mat_Acoustic cost effective compared to other formulations [8].

2.5.1.1 Timestep

A sufficiently small timestep needs to be chosen in order to guarantee stability of the system. For Mat_acoustic the timestep is affected by three variables; L , the smallest cross dimension of a fluid-volume finite element, c , the acoustic velocity of water and β , the damped integration coefficient.

First, the smallest timestep fulfilling the Courant-Friedrichs-Levy (CFL) condition is defined. The Courant condition states that the timestep must be sufficiently small in order to guarantee that information does not travel faster than the timestep times the smallest distance between two nodal points. The Courant timestep h_c can be expressed as

$$h \leq h_c = L/c \quad (2.31)$$

Second, the stability effect of the damped integration factor β must be taken into consideration. From analysis presented in [2] it can be shown that the largest possible timestep guaranteeing stability is

$$h_{max} = \frac{h_c}{\sqrt{1+2\beta}} \quad (2.32)$$

2.5.1.2 Mesh Size

For Mat_Acoustic there are two ways to couple the structure with the fluid. Either the nodes of the structure are coincident with the nodes of the acoustic fluid or a mismatch coupling must be used in LS-DYNA. The following condition must be satisfied for the fluid-structure coupling to be stable:

$$\frac{2\rho_a D}{\rho_s t_s} < 5 \quad (2.33)$$

where ρ_a is the density of the acoustic medium, D is the thickness of the acoustic elements closest to the structure, ρ_s is the density of the structure and t_s is the thickness of the structural elements [11]. If the structural elements are solids or thick shells, t_s should be set to half the thickness of the elements. Furthermore, if both sides are coupled, then t_s should be half the element thickness. Apart from the condition stated in (eq. 2.33) convergence studies are performed to determine the required fluid mesh size in order for the solution to converge.

2.5.2 Displacement Potential

The displacement potential Ψ is the potential field whose gradient is the displacement.

Let $X = (X, Y, Z)$ be the global-coordinate vector. Then $x = x(X)$ is the fluid-particle displacement field under dynamic conditions.

The fluid particle displacement u relative to a reference hydrostatic displacement x^H is then defined as

$$u = x - x^H \quad (2.34)$$

Displacement potential Ψ is then a scalar potential defined by

$$\nabla \Psi = -\rho u \quad (2.35)$$

By using displacement potential as the primary variable calculations per time step are almost trivial as only one degree of freedom has to be computed [11]. To clarify, the hydrostatic displacement is the displacement caused by the hydrostatic pressure. In the FE-model, $x^H = 0$, as there is no hydrostatic pressure due to the assumption of no gravity.

2.5.3 Acoustic Wave Equation

In fluid structure interaction problems usually both the displacement u and the pressure p are wanted. Solving the wave equation for u does not always provide p and vice versa. However by introducing the wave displacement potential, solving it will provide both u and p .

Acoustic wave equation of displacement potential, Ψ [4]

$$\nabla^2 \Psi - \frac{1}{c^2} \frac{\partial^2 \Psi}{\partial t^2} = 0 \quad (2.36)$$

which yields u and p from

$$p = -\frac{\partial^2 \Psi}{\partial t^2} = \nabla^2 \Psi c^2 \quad (2.37)$$

and

$$u = \nabla \Psi \quad (2.38)$$

Note that use of a displacement potential enforces flow without rotation as

$$\nabla \times u = \nabla \times \nabla \Psi = 0 \quad (2.39)$$

2.6 Concept of Added Mass

When a structure accelerates in a fluid kinetic energy is not only increased due to the movement of the structure. Fluid in contact with the structure is also accelerated resulting in that work associated with the kinetic energy of the accelerated fluid also has to be taken into account. This additional kinetic energy, T , can be represented by

$$T = \frac{\rho}{2} \int_V (u_1^2 + u_2^2 + u_3^2) dV = \frac{\rho}{2} \int_V u_i u_i dV \quad (2.40)$$

where $u_i (i = 1, 2, 3)$ represent the Cartesian components of the velocity and V is the volume containing the fluid. As water is incompressible, ρ can be considered constant. Considering the motion of the body to be of a straight line nature through fluid otherwise at rest it is clear that the kinetic energy, T , is constant in time. Additionally it is clear that the kinetic energy of the fluid is proportional to the square of the velocity, U , of the body. If this indeed is the case in addition to the fact that a change of U will result in a change of direct proportion in u_i . The kinetic energy T can then be expressed as

$$T = \rho \frac{I}{2} U^2 \quad \text{where} \quad I = \int_V \frac{u_i}{U} \frac{u_i}{U} dV \quad (2.41)$$

where I is an invariant. This formulation holds for low Reynolds number Stokes flow. However at complex flows or flows at intermediate Reynolds numbers this may no longer be true. To accelerate the body, the rate of additional work required with respect to time can be stated as dT/dt . This means that the acceleration of the fluid can be seen as a drag force, F , such that $-FU$ simply equals dT/dt . If the flow stays the same I remains constant and thus it follows that the added drag force F is

$$F = -\frac{1}{U} \frac{dT}{dt} = -\rho I \frac{dU}{dt} \quad (2.42)$$

This formulation of F has the same form as the force required to accelerate the body, $m \frac{dU}{dt}$. It is from this similarity that the accelerated fluid mass, ρI , can be seen as an "added mass" to the system. Note that there in reality is no such mass being accelerated to the same degree as the body however this is an efficient abstract simplification [1, p. 2-3].

2.6.1 Natural Frequency in Fluid

Previously the natural frequency has been shown to equal (eq. 2.4)

$$\omega_n = \sqrt{\frac{k}{m}} \quad (2.43)$$

However, when accounting for the additional inertia of the system due to the displacement of the surrounding fluid an added mass force is added to the equation of motion, eq. 2.2

$$(m + m_a) \ddot{x} + kx = 0 \quad (2.44)$$

where m_a is the added mass. With the addition of added mass the system can now be treated as a regular spring-mass system and the natural frequency becomes

$$\omega'_n = \sqrt{\frac{k}{m + m_a}} \quad (2.45)$$

2.6.2 Analytical Solution for Added Mass

The concept of added mass provides a simple and efficient method of dealing with accelerating structures interacting with fluids. The only challenge is calculating the appropriate added mass for a specific structure. For simple geometries there are a few analytical solutions; however there are no analytical solutions for complex geometries.

For an idealized flow past an infinite thin plate accelerated normal to its surface the added mass can be assessed as the mass of a cylinder with the height and diameter of a side length[1, p. 5].

$$m_A = \frac{\rho s^3 \pi}{4} \quad (2.46)$$

where s is the side length of a square plate. In this report analytic added mass is calculated according to (eq. 2.46). It is also common practice to assess the added mass as a sphere instead of a cylinder, see (eq. 2.47).

$$m_A = \frac{\rho s^3 \pi}{6} \quad (2.47)$$

3 Experiments

3.1 Experimental Setup

In order to investigate the fluid-structure interaction, an experimental rig was built and used in a water tank. The rig consisted of a frame, a box and a plate (fig. 3.1 & 3.2). The frame provided the experiment with a stable submerged structure from which an object could be fastened.

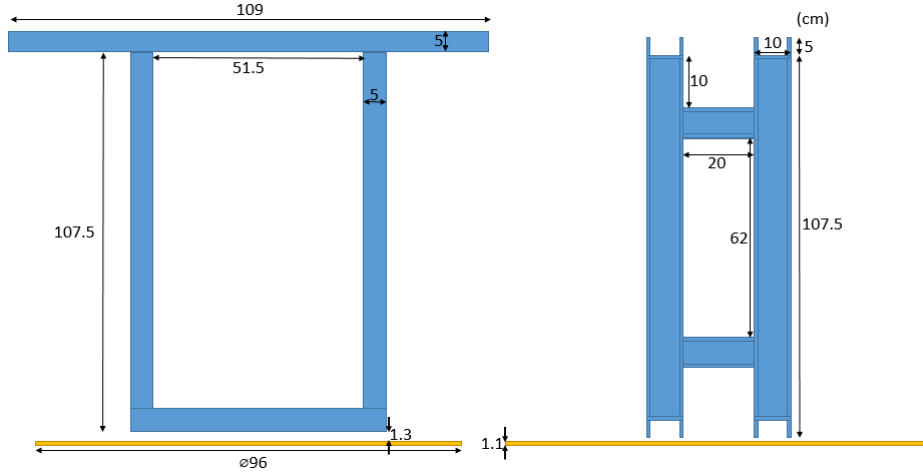


Figure 3.1: The conceptual drawing of the frame (blue) and the plate (yellow). The profile used for the frame was UNP100.

A metal box was constructed and used as the structure interacting with the water. The box was mounted on four springs (fig. 3.3) on the frame which allowed it to oscillate freely.

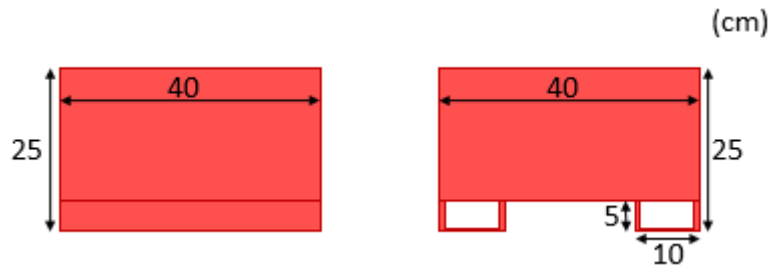


Figure 3.2: The conceptual drawing of the box. The springs were mounted on the u-shaped feet at the bottom of the box. The box's sides were 5 mm thick.

In order to investigate changes of the fluid dynamics a plate was constructed which could be mounted below the frame. The plate provided the experiment with an optional increase of fluid structure interaction by hindering the flow of water. The plate can be seen in yellow in figure (3.1). A key goal in the setup of the experiment was to reduce all oscillations except the vertical translation as this was the motion of interest. To reduce unwanted translational and rotational oscillations the two springs with the highest stiffness were placed diagonally.



Figure 3.3: Here the box is mounted on the frame with the tank in the background and wires connected to the measuring devices.

The box was lifted via four wires originating from its corners which is illustrated in figure (3.4). Each wire was in turn connected to a turnbuckle and then to each other above the center of the box. To achieve an even lift the length of the turnbuckles could be adjusted. The entire setup was then via a series of crane slings attached to a traverse crane in the ceiling of the building. The crane provided the initial offset of the springs which would allow the box to oscillate upon release.

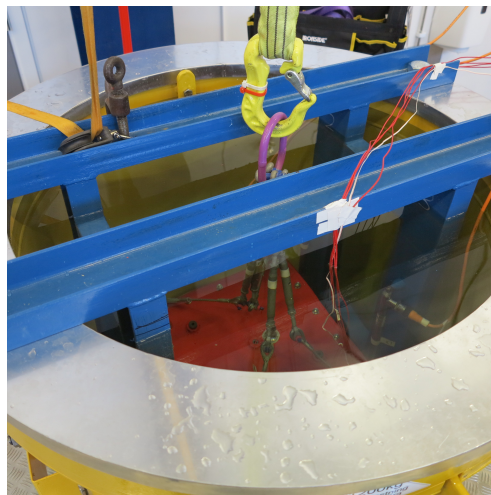
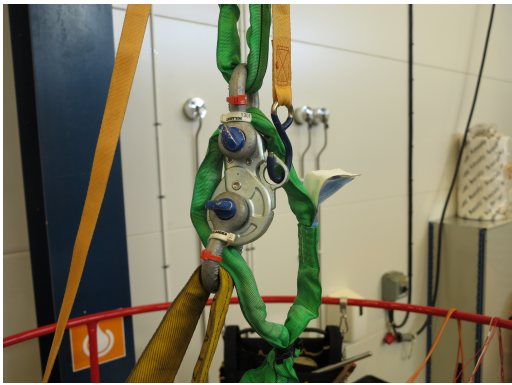


Figure 3.4: The frame and the box are submerged under water and the pull mechanism is in place

The release mechanism is illustrated in figure (3.5) and consisted of a rope attached to a release hook. Pulling the rope released the set of crane slings attached to the wire ropes. The release mechanism was placed as far away from the box as possible to reduce the error from misalignment. In the picture a slack catch-loop can also be seen. This loop was put into place in order to prevent the lifting arrangement from falling on top of the box which would have interfered with the oscillation.

The rope attached to the hook went all the way down to the tank and redirect by a pulley so that it was possible to pull the rope horizontally while still pulling the hook vertically.



(a) Loaded



(b) Released

Figure 3.5: Pulling the yellow rope released the hook. The green crane sling makes sure the rest of the slings only fall a short distance.



Figure 3.6: The traverse crane at the top of the picture is connected to the submerged box via a set of crane slings

3.1.1 The Design of The Box

The box was made out of 5mm thick steel and painted to avoid rusting. The lid could be removed. To avoid leakage the box was sealed using a type of plastic cover (fig. 3.7). Furthermore, shackles could be attached to the corners on the top of the box in order to lift the box. Pressure gauges and accelerometers were attached to the center of the lid and the bottom of the box. The pressure gauges had to be connected to the computer via wires and an additional hole was thus needed which was placed on one of the side walls. The hole was sealed with clay. Furthermore, the connection between the gauges and the wires had to be sealed with clay as the connection was not water proof. The position sensors were fastened to the side of the box and the frame (fig. 3.7).

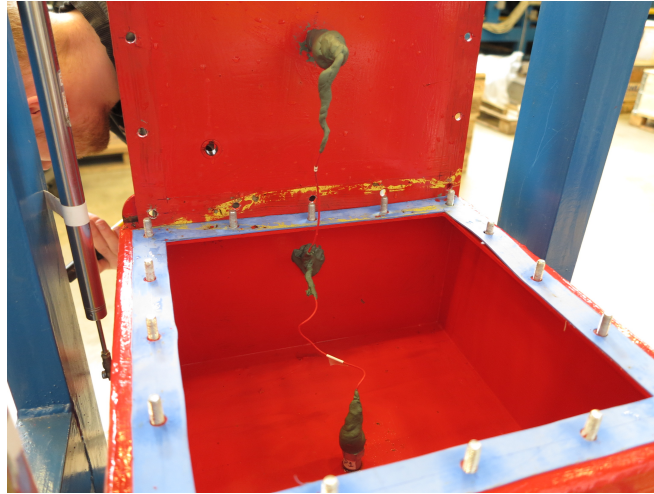


Figure 3.7: The blue plastic cover was used to prevent leaking when the empty box was submerged. The gray clay sealant was used to protect the gauges from the water. The gauges are connected to the computer via red wires.

3.1.2 Measuring Devices

The measuring devices used in the experiment were accelerometers, pressure gauges, position sensors and a strain gauge. The placement of the measuring devices can be seen in (fig. 3.8) where PS are the position sensors, P - the pressure gauges, A - the accelerometers and S the strain gauge. The gauges at the bottom are placed in the same manner as the gauges at the top except there is no strain gauge at the bottom.

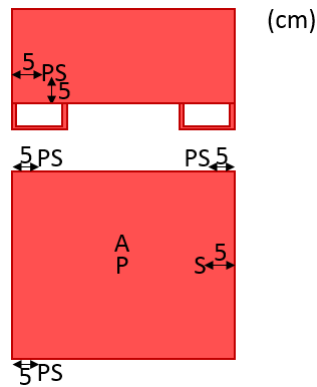


Figure 3.8: The drawing at the top is the box from the side, depicted below is a view of the box from above.

The accelerometers were piezoelectric which yielded an electric discharge per ms^{-2} . The charges from the accelerometers were connected to a charge amplifier which converted the electrical charge into a voltage (3.9). The charge amplifiers were in turn connected to a data acquisition unit which converted all the analog signals into digital signals (fig. 3.10). The data acquisition unit was connected to a computer where the digital signals were saved and analyzed in an experimental software. The pressure gauges were also piezoelectric and connected in the same manner as the accelerometers. The position sensors were always fastened 5 by 5 centimeters from a bottom corner.



Figure 3.9: The charge amplifiers used by both the accelerometers and the pressure gauges were connected to the data acquisition unit.

The position sensors were linear variable displacement transformers which converted an input voltage depending on the displacement. The output voltage from the position sensors was amplified and then plugged into the data acquisition unit. The strain gauge could measure strain in one direction and used a Wheatstone bridge in order to amplify small changes in resistance due to material strain.



Figure 3.10: The data acquisition unit makes pleasurable clicks when you turn it on click click click click.

3.2 Experimental Procedure

In order to increase the quality of the results all equipment were first carefully weighed and calibrated. The heavy objects were weighed using a dynamometer with an approximate tolerance of 100 g and the smaller objects such as screws and measuring devices were weighed on a scale with a tolerance of 1 g. The scales were never calibrated further than observing that there were no offset errors. The position sensors were calibrated using an electronic caliper and it was noted that the highest accuracy was when the displacement was half of the maximum displacement available. The position sensors also added some mass to the box which was included in all calculations.

The accelerometers and pressure gauges used were recently calibrated by Kockums. Furthermore the accelerometers were initially placed next to the position sensors and the double integration of the acceleration was the same as the displacement from the position sensors when the acceleration was filtered through a high pass filter.

The springs were measured in a tensile tester, yielding values of the spring constants in both tension and compression. After calibrating the equipment, the springs and the box were mounted onto the frame with spacers. The spacers were added to make sure that the maximum difference in

length between the springs were 2 mm . The frame was then lowered into the tank. The water level in the tank was raised to a level where it no longer affected the motion of the box. A motivation for the chosen water level is presented in 3.7.1

The frame was fastened to the tank and the crane was centered using a folding ruler. The measuring devices were zeroed out and the box was lifted without the release mechanism. The positions were noted and the turnbuckles were adjusted iteratively in order to lift the box as evenly as possible; the largest acceptable difference between two position sensors was 2 mm . The release mechanism was then mounted onto the crane and the box was lifted 20 mm which was controlled using the position sensors. The collection of data was then initialized and the release mechanism was triggered using the rope which was attached to the hook.

The experiments were performed using two different types of springs. The mass of the box could also be altered by filling it with water. These adjustments yielded four different experimental setups aimed to change the natural frequency. For each setup there were three different experiments to be performed: in air, in water and in water with a plate. All in all this produced 12 different experiments which are presented in table (3.1). Here the number indicates the combination of spring constant and mass, and the letter a means that the experiment took place in air, w - in water and p - in water with a plate.

Table 3.1: The total spring constant and the mass of the box were used together with the analytical added mass (sec. 2.6.2) to calculate an analytic frequency (eq. 2.45). A third of the mass of the springs is included in m_{Box}

Lc	k_{Total} [kN/m]	m_{Box} [kg]	$f_{Analytic}$ [Hz]	m_{Added} [kg]
1_a	154.4	35.6	10.5	0
2_a	154.4	64.6	7.8	0
3_a	281.6	36.0	14.1	0
4_a	281.6	65.0	10.5	0
1_w	154.4	35.6	6.7	50.3
2_w	154.4	64.6	5.8	50.3
3_w	281.6	36.0	9.1	50.3
4_w	281.6	65.0	7.9	50.3
1_p	154.4	35.6	6.7	50.3
2_p	154.4	64.6	5.8	50.3
3_p	281.6	36.0	9.1	50.3
4_p	281.6	65.0	7.9	50.3

Initial experiments in air showed that the mass of the springs could not be neglected after comparing the analytical and measured frequency. The effective mass of an ideal uniform spring can be derived to be one third of the mass of that spring. The mass of the springs were measured and one third was added to the mass of the box.

3.2.1 Sources of Error and Assumptions

The initial conditions of the oscillation are critical to the overall quality of the measurement. A purely translational motion is desirable and anything which could introduce rotational modes is of concern. During the release of the box, the ropes in which the box was suspended were pulled horizontally. Horizontal displacements of the ropes pulling the box could occur during release. This would in turn alter the angle at which the box was being pulled.

Another problem was the centering of the pulling force. This was an issue as the force was to be divided into four equal parts at each corner. This proved difficult as the central pulling force was not perfectly in the center above the box. The wires attached to the corner were also not necessarily of the same length. The turnbuckles made it possible to reduce this effect..

The interpolation of the displacement eliminated rotational modes around the center of the box. Rotational modes around the sides of the box were not eliminated, nor could they be reduced.

The horizontal stiffness of the springs constricted translational modes in the horizontal directions. Rotational modes can form as a result of varying spring constants. The springs were measured by a tensile tester with a high degree of accuracy and the largest difference was 2.5% for the weak springs and 1% for the strong springs. To minimize rotational modes the stiffest springs were placed diagonally.

The experiments in air were conducted without some of the gauges that were used in water, this altered the mass. All components attached to the box were included in the box's mass but there were some sources of errors for the mass. The weight of the pull arrangement was not included in the box's mass and the effective mass of the springs was also an approximation.

Regarding the pressure gauge and the accelerometer no calibration took place as they had recently been calibrated by Kockums. An issue was that water could seep through the sealant and affect the measuring devices. This would render the device useless but the upside was that it was easy to detect. This happened to one of the pressure gauges which is why some of the measurements only contain one pressure.

3.3 Experimental Results in Air

Measurements of the same quantities were taken in air and water. However as it is the fluid structure interaction that is to be investigated only the displacement is presented in this section. The displacement is measured by averaging the data from two diagonal position sensors (fig. 3.11).

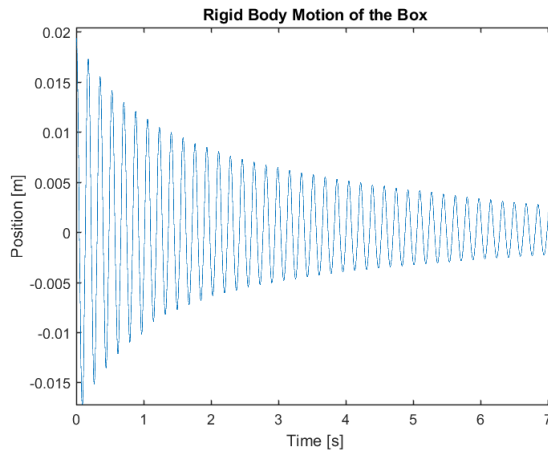


Figure 3.11: The displacement was interpolated from two diagonal position sensors so that the displacement in the center could be calculated.

It is from the measurement of the displacement that the frequency was calculated. The average frequency of a measurement was calculated by averaging a set of wavelengths in the middle of the sample. The frequencies for all the different experiments in air are presented in table (3.2).

Table 3.2: Not much variation can be observed within a case.

1_a	f [Hz]
Trial 1	10.57
Trial 2	10.58
Trial 3	10.57
2_a	f [Hz]
Trial 1	7.76
Trial 2	7.76
3_a	f [Hz]
Trial 1	13.89
Trial 2	13.89
4_a	f [Hz]
Trial 1	10.44
Trial 2	10.44
Trial 3	10.44

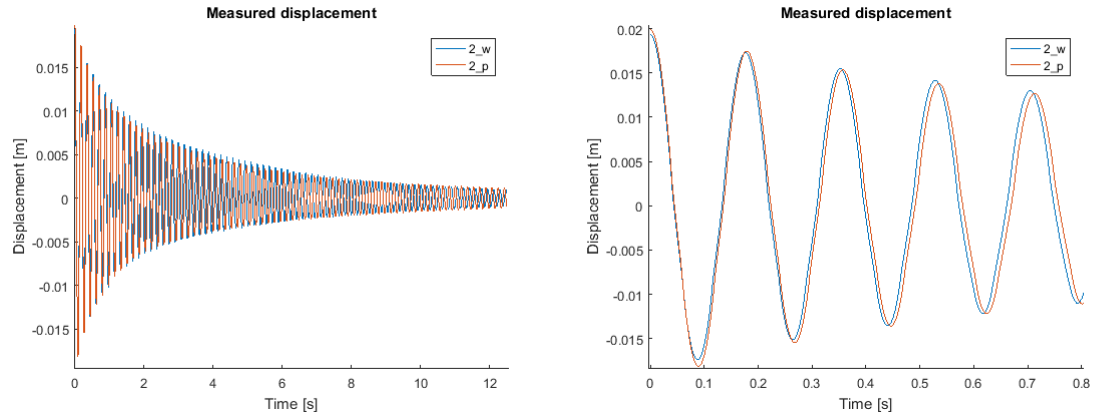
3.4 Experimental Results in Water

There were four different combinations of springs and masses for the box and each experiment was conducted with and without the bottom plate in place. In this section the results for one

setup with and without the plate are presented. The chosen setup is using the weaker springs and the heavier mass, 2_w & 2_p. In order to compare the effects of the addition of the plate both measurements are plotted in the same figure.

3.4.1 Displacement

The displacement was measured by averaging the data from two diagonal position sensors (fig. 3.12). The results are similar with and without the plate although a small change of frequency occurs.



(a) The evolution of the displacement is similar with or without the plate.

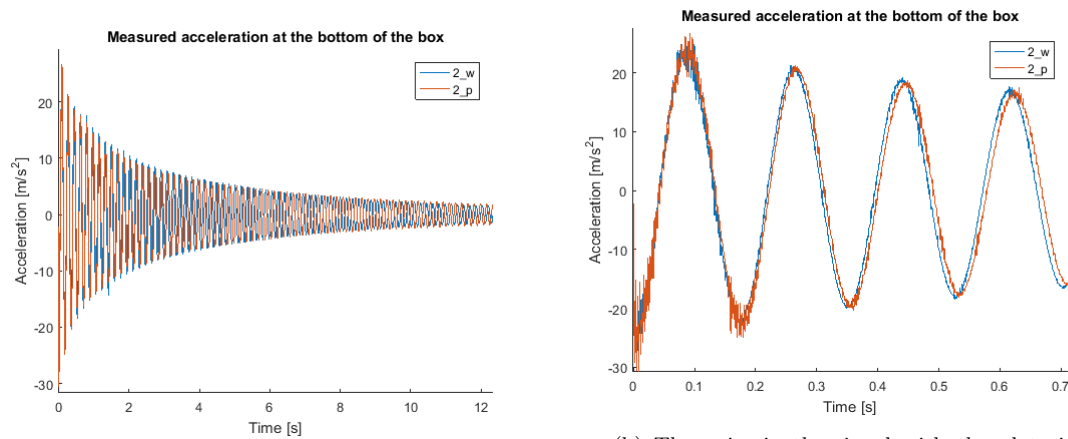
(b) When taking a closer look the frequency is slightly decreased when the plate is added.

Figure 3.12: The starting amplitude is typically $0.02m$ and then decays in a nonlinear fashion.

With the addition of the plate the frequency decreases due to an increase of added mass.

3.4.2 Acceleration

The acceleration is measured at the top and bottom centre of the box (fig. 3.13 & 3.14). At the bottom of the box accelerations are initially higher with the plate.

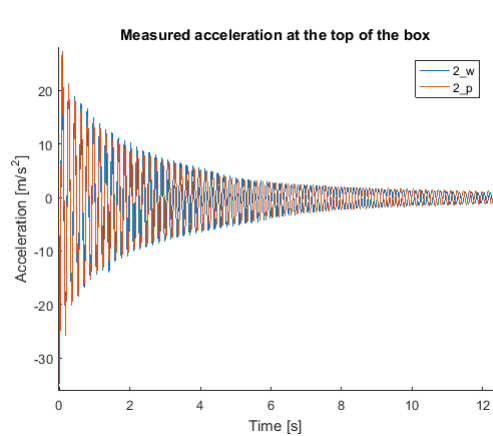


(a) The acceleration at the bottom of the box is similar with and without the plate.

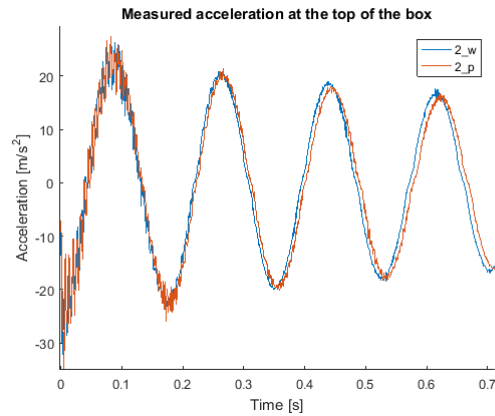
(b) The noise in the signal with the plate is initially higher compared to the signal without the plate. Otherwise they are of similar amplitudes starting at around $23m/s^2$ and then decreasing.

Figure 3.13: The acceleration is defined as positive upwards. The frequency with the plate is slightly lower compared to without the plate

The accelerations at the top are initially higher but after one wavelength the signals coincide except for a small change of frequency.



(a) The acceleration at the top of the box is similar with or without the plate.

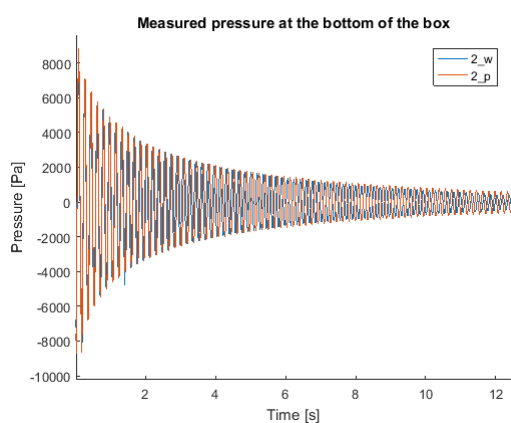


(b) The noise in the signal with the plate is initially higher compared to the signal without the plate. Otherwise they are of similar amplitudes starting at around 25m/s^2 and then decreasing.

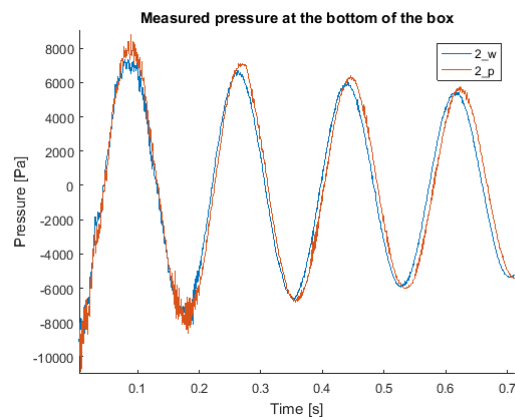
Figure 3.14: The acceleration is defined as positive upwards. The frequency with the plate is slightly lower compared to without the plate

3.4.3 Pressure

The pressure is measured at the bottom center of the box (fig. 3.15).



(a) The evolution of the pressure is similar with or without the plate.



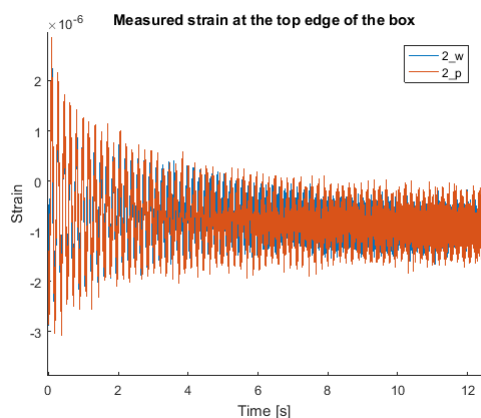
(b) The signal with the plate contains more noise and is of higher values than the one without a plate.

Figure 3.15: Depicted is the dynamic pressure.

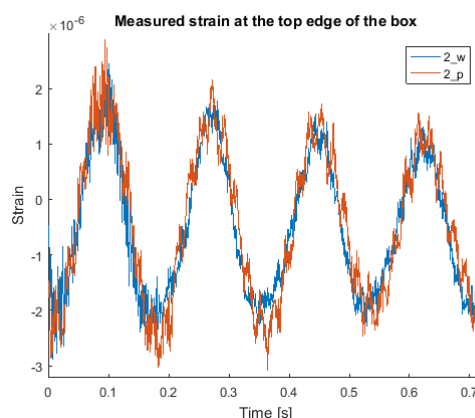
The pressure at the bottom of the box contains more noise and higher values when the plate is introduced. The gauge placed at the top was not working properly and its data is therefore not presented.

3.4.4 Strain

The strain is measured at the top surface, in the middle approximately 5 cm from the edge (fig. 3.16).



(a) As strains are low, noise has high influence on the measurement. With time the wave does not oscillate around zero.



(b) Initially the strain wave can clearly be seen although there is a lot of high frequency noise.

Figure 3.16: It can be observed that the strain oscillates with the same frequency as the rest of the box.

In the end of the signal the center is no longer around zero as it should be since the signal was zeroed before the experiment. This is due to a problem with the strain gauge causing it to drift over time. It can be observed that the strain oscillates with the same frequency as the rest of the box.

3.5 Added Mass

From the calculated frequency, the known mass and the spring constants; added mass was calculated for each experiment from eq. (2.45). The added mass for each trial is presented in table (3.3)

Table 3.3: The left table presents the frequency and added mass for the four cases and all trials without the plate. The right table presents the same cases with the plate. The added mass was calculated from eq.(2.45)

1_w	f [Hz]	m_a [kg]
Trial 1	6.53	56.0
Trial 2	6,53	56.1
2_w	f [Hz]	m_a [kg]
Trial 1	5.69	56.0
Trial 2	5.70	56.0
3_w	f [Hz]	m_a [kg]
Trial 1	8.74	57.3
Trial 2	8.74	57.3
Trial 3	8.74	57.3
4_w	f [Hz]	m_a [kg]
Trial 1	7.63	57.4
Trial 2	7.63	57.7
Trial 3	7.62	57.7

1_p	f [Hz]	m_a [kg]
Trial 1	6.45	58.5
Trial 2	6.44	58.8
Trial 3	6.45	58.4
2_p	f [Hz]	m_a [kg]
Trial 1	5.64	58.5
Trial 2	5.63	58.8
Trial 3	5.64	58.5
3_p	f [Hz]	m_a [kg]
Trial 1	8.65	59.3
Trial 2	8.65	59.2
Trial 3	8.65	59.3
4_p	f [Hz]	m_a [kg]
Trial 1	7.57	59.6
Trial 2	7.57	59.4
Trial 3	7.57	59.6

As can be seen in table (3) added mass remains constant for each type of spring. The added mass is heavier for the larger spring constants.

With the addition of the plate added mass increased by $2.5kg$ for the weaker springs and $2kg$ for the stiffer springs. The results from the different mass spring setups are averaged in table (3.4).

Table 3.4: The two tables present the added mass with and without the plate calculated as averages of the different trials.

	f [Hz]	m_a [kg]		f [Hz]	m_a [kg]
1_w	6.53	56.1	1_p	6.44	58.6
2_w	5.70	56.0	2_p	5.63	58.6
3_w	8.74	57.3	3_p	8.65	59.3
4_w	7.63	57.6	4_p	7.57	59.5

Here it can be clearly seen that added mass increased with stiffer springs and with the addition of the plate.

3.6 Summation of Results

The results from the analytical solutions, experiments in water and air are presented in table (3.5).

Table 3.5: The analytical added mass is constant between the cases and appears to be independent of the natural frequency. The measured experimental results are presented next to the analytical results.

Lc	k_{Total} [kN/m]	m_{Box} [kg]	$f_{Analytic}$ [Hz]	m_{Added} [kg]	$f_{Measured}$ [Hz]	m_{Added} [kg]
1_a	154.4	35.6	10.47	0	10.57	0
2_a	154.4	64.6	7.78	0	7.76	0
3_a	281.6	36.0	14.07	0	13.89	0
4_a	281.6	65.0	10.48	0	10.44	0
1_w	154.4	35.6	6.75	50.3	6.53	56.1
2_w	154.4	64.6	5.83	50.3	5.70	56.0
3_w	281.6	36.0	9.09	50.3	8.74	57.3
4_w	281.6	65.0	7.87	50.3	7.63	57.6
1_p	154.4	35.6	6.75	50.3	6.44	58.6
2_p	154.4	64.6	5.83	50.3	5.63	58.6
3_p	281.6	36.0	9.09	50.3	8.65	59.3
4_p	281.6	65.0	7.87	50.3	7.57	59.5

The analytical frequencies were close to the frequencies from the experiments in air but differed most for 3_a where the analytical frequency was 1.3 % higher than the experimental value.

The added mass for 1_w and 2_w were similar and used the same springs, the same holds for 3_w and 4_w but with a higher added mass. This was also true for the cases with the plate. The largest differences in added mass were 3 % without the plate and 2 % with the plate. Furthermore, it can also be observed from table (3.5) that the added mass increased when the plate was introduced. The largest difference was observed for case 2 where the added mass of 2_p was 5 % higher than for 2_w. The remaining cases differed by at least 3 %. Moreover, the experimental added mass for 4_w was 15 % higher than the analytical added mass which was the largest difference. The smallest difference in added mass was observed for 2_w which was 11 % higher than the analytical. For the plate, the added mass for 4_p was 18 % larger and for 1_p it was 17% larger. Keep in mind that for these results the analytical added mass is assessed as a cylinder, if a sphere was to be used instead the assessment would be 33% lower.

3.7 Validation of Results

In order to assess the quality of the measurements a validation of the results and the experimental setup was performed. In the measurements, the frequency is considered the most important variable. It is calculated as the average time for the displacement to change sign 9 times. This provides a robust but still time dependent measurement of the frequency. When the frequency is noted as a single number the average is calculated for the middle of the signal.

3.7.1 Influence of Water Level

Results where an infinite water pillar can be assumed are desired as that would make the results more general. In order to rule out the effect of having a limited water pillar above the box, tests

were made with different heights of water. From the tests the frequency of the displacement was measured and considered a significant variable for controlling overall change. If the frequency did not change when the water level was raised, the assumption of infinite water height was considered to hold.

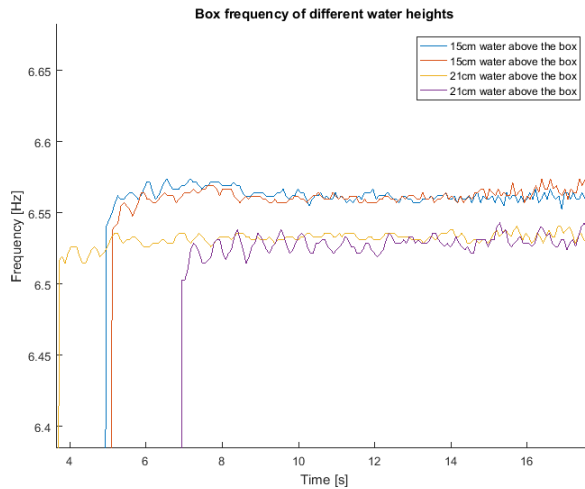


Figure 3.17: A clear change of the frequency can be seen as the water level is raised to 21cm compared to a height of 15cm above the box. The different starting times are due to measurements starting before the box was released.

As can be seen in fig. (3.17) using a water level of 15cm above the box does not satisfy the assumption of infinite water height as the frequency is not constant.

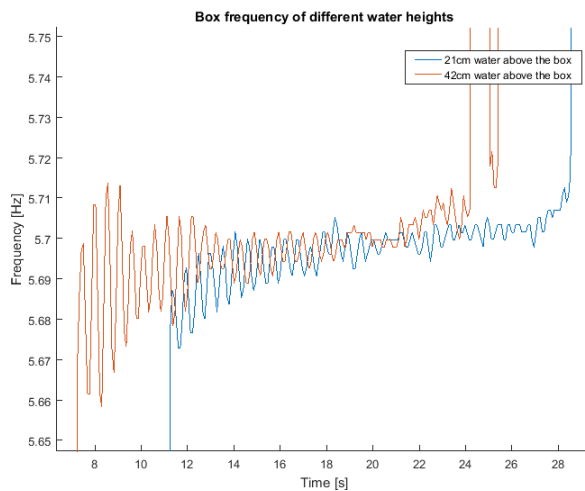


Figure 3.18: As the water height was increased to 42cm from 21cm the change of frequency became small.

From the increase of 6 cm in figure (3.17) the change of frequency can clearly be seen. When regarding the figure (3.18) where a larger difference in water height, 21 cm, takes place the effect on the frequency becomes insignificant. From these tests it can be concluded that an increase in water height eventually has no influence on the frequency of the box. This occurs in a nonlinear fashion however further testing has to take place in order to determine the mechanics behind this phenomenon. In the experiments performed, a water height of 42 cm above the box was used. The above tests are empirical evidence that show that an infinite water height can be assumed for the results attained. Furthermore the experimental setup made it unpractical to raise the water level further.

3.7.2 Influence of Amplitude

In order to decide at what height the box should be released at, tests had to be performed. Three different tests were conducted using amplitudes of 20, 10 and 5mm with an otherwise identical experimental setup. In addition a ratio between the largest and the second largest rotational or translational mode was created. The ratio was introduced in order to quantify the quality of a measurement. A large ratio was desirable as it meant that the translational mode which we are interested in is large compared to other modes which might interfere with our measurements.

Table 3.6: With higher amplitude the ratio increases according to these measurements. The frequency remained constant

Amplitude	Analytical eigenfreq.	Measured eigenfreq.	Ratio between largest modes
5mm	10,491 Hz	10,573 Hz	2,624
10mm	10,491 Hz	10,583 Hz	4,055
20mm	10,491 Hz	10,565 Hz	4,623

From table (3.6) it can be seen that the most accurate frequency compared to the analytical solution is when using 20 mm amplitude. Furthermore the largest ratio is measured when using the largest amplitude. It should also be stated that the data contained in the smaller starting amplitude waves can be considered to be part of the largest starting amplitude wave as amplitudes for a 20 mm wave will eventually become 10 mm and 5 mm as the wave decays. From this analysis it was concluded that all experiments should be performed using 20 mm as the initial amplitude. Even larger initial amplitudes would be desirable however the springs will deform plastically at 30 mm making it unpractical.

3.7.3 Verification of Acceleration and Displacement

The acceleration of the box was measured at the top and bottom and will in this section be used to verify that the measured acceleration and displacement yield similar results for 1_w.

The plotted accelerations in fig. (3.19) illustrates that the phases are indeed similar. However, it turns out the acceleration on the top of the box decays faster than on the bottom which could be due to the oscillation of the lid.

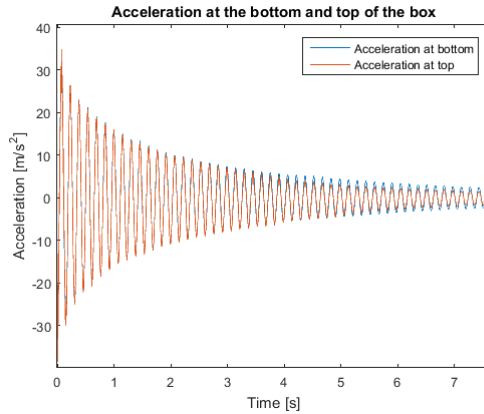


Figure 3.19: The two accelerations are in phase but slightly different in amplitude as time progresses.

The accelerations were integrated twice which yielded the displacement of the box (fig. 3.20). A Butterworth high-pass filter was used to eliminate drifting errors.

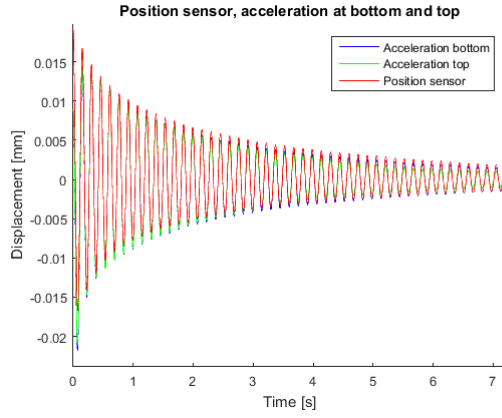


Figure 3.20: Illustrates the measured displacement of the box as well as the two computed displacements. The frequency of the motion is similar for the three sensors.

There is yet again some difference in amplitude between the two accelerometers as well as the position sensors which could be due to the box not being a rigid body. Nevertheless, they are in-phase with one another. In order to verify that the accelerometers and the position sensors yield the same frequency, the different frequencies were plotted in (3.21).

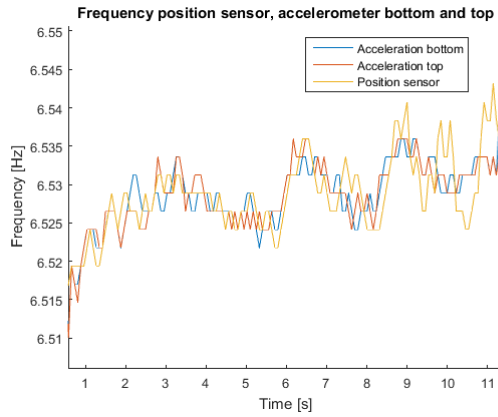


Figure 3.21: The three frequencies plotted as running averages over 9 wavelengths. The frequencies follow each other closely.

The frequency can also be plotted in the frequency domain which yielded a similar value (fig. 3.22).

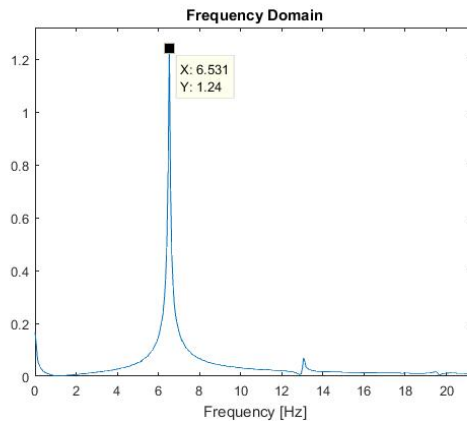


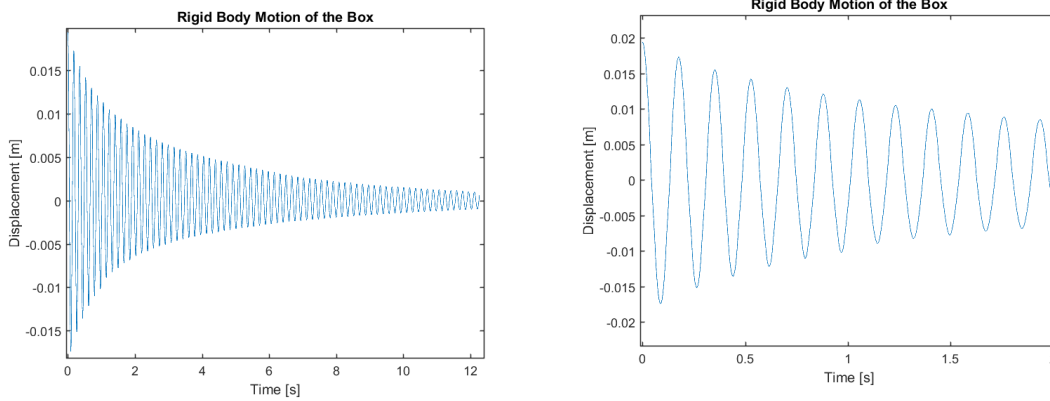
Figure 3.22: Here, the motion of the position sensor is transformed into the frequency domain using an FFT.

As evidenced by figure (3.21), all three frequencies are almost identical and the measurements

are therefore satisfactorily similar. The calculated frequencies are based on displacement and not acceleration in this report.

3.7.4 Decay

It is evident from the experiments that the oscillating motion of the box is subjected to damping (fig. 3.23).



(a) The motion continues to decay over the entire time span.

(b) An image zoomed in for the first 10 peaks better illustrates the behavior of the damping at the start.

Figure 3.23: (a) illustrates decay for 2_w and (b) illustrates the decay for the first 10 peaks.

Values for the 10 first peaks for a 2_w experiment (fig: 3.23b), not including the starting displacement, were observed and presented in table (3.7). The first peak was not included as it may have been affected by disturbances when the motion was initialized.

Table 3.7: The amplitudes can be used to calculate the damping ratios.

Amplitude (mm)	17.3	15.5	14.2	13.0	12.1	11.3	10.5	9.9	9.4	8.8
----------------	------	------	------	------	------	------	------	-----	-----	-----

The values in table (3.7) were inserted into equation (2.11) to calculate the damping ratios (table 3.8).

Table 3.8: The calculated damping ratios decrease as the motion decays over time. Note that the ratio decreases with time, meaning that the damping decreases.

ζ	0.0173	0.0142	0.0138	0.0116	0.0110	0.0117	0.0083	0.0087	0.0099
---------	--------	--------	--------	--------	--------	--------	--------	--------	--------

It has previously been discussed that the damping affects the natural frequency. This poses the question as to whether this effect is significant or not. Equation (2.6), can be used to calculate the damped frequency for the highest damping ratio.

$$f_d = 0.99985f_n$$

The difference between the damped frequency and the natural frequency is considered too small to be relevant.

The damping can be described as an exponential function that corresponds to the envelope of the signal. The envelope was generated with the MATLAB command *envelope*, and an exponential curve on the following form was generated with *cftool* in MATLAB

$$f(t) = ae^{bt} \tag{3.1}$$

where a is the starting amplitude and t is the time. Generally, the decay of the sinusoidal wave's envelope can be expressed as an exponential function but it was not possible for the entire signal

as evident from fig. (3.24a). It was however possible to find a better fit for the first 1.6 seconds (3.24b) with the following constants:

$$a = 0.01846 \text{ m} \quad b = -0.459 \text{ s}^{-1} \quad (3.2)$$

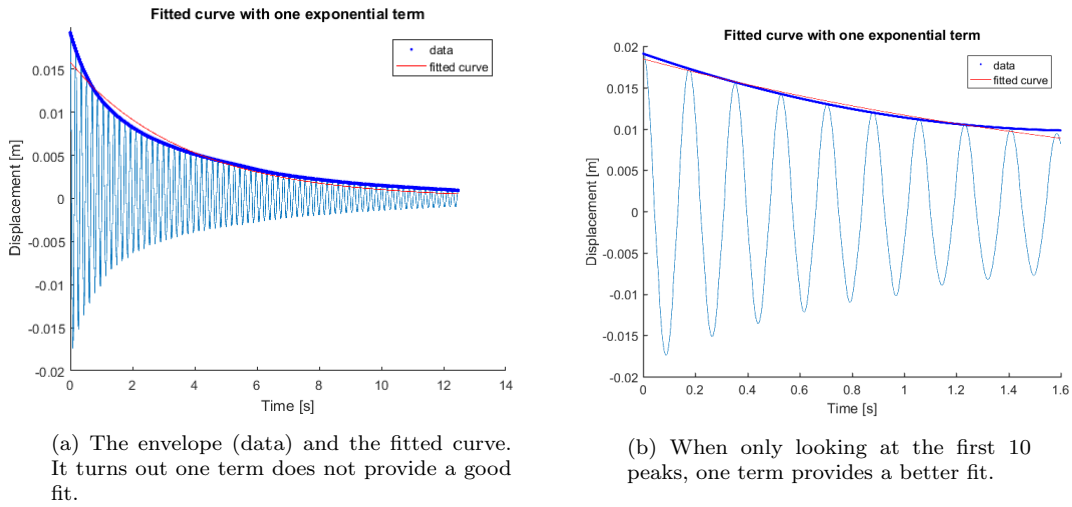


Figure 3.24: The decay and a fitted curve with one exponential term for the entire signal (a) and the beginning (b).

To get a better fit for the entire signal, a second term was added to the exponential function resulting in (3.3) with constants presented in eq. (3.4). The fitted curve is shown in fig. (3.25).

$$f(t) = ae^{bt} + ce^{dt} \quad (3.3)$$

with the following constants

$$a = 0.007603 \text{ m} \quad b = -1.344 \text{ s}^{-1} \quad c = 0.01166 \text{ m} \quad d = -0.207 \text{ s}^{-1} \quad (3.4)$$

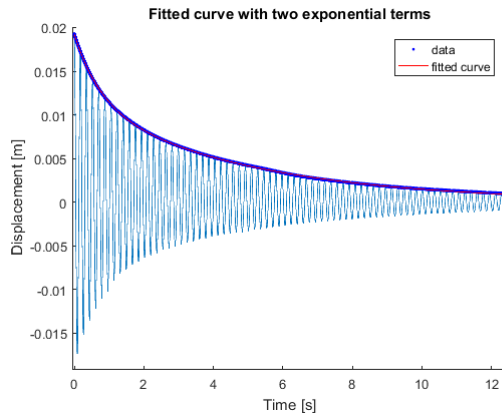


Figure 3.25: Two exponential terms yields an exponential function that much better fits the envelope.

The same analysis was performed for all the different cases and the constants are presented in table (3.9) and (3.10). It should be noted when interpreting the data that some of the constants may be highly dependant on the starting amplitude. Constants a and c should together be equal to the starting amplitude.

Table 3.9: Generated constants for the four different cases without a plate. Some variation can be observed even within the same case, for example for 1_w and 3_w.

1_w	a	b	c	d
Trial 1	0.0094	-1.42	0.00878	-0.1878
Trial 2	0.008349	-1.722	0.01072	-0.2564
2_w	a	b	c	d
Trial 1	0.007603	-1.344	0.01166	-0.207
Trial 2	0.008009	-1.386	0.01201	-0.2037
3_w	a	b	c	d
Trial 1	0.01137	-1.868	0.008297	-0.2782
Trial 2	0.01193	-1.595	0.006681	-0.206
Trial 3	0.01557	-2.232	0.005803	-0.5629
4_w	a	b	c	d
Trial 1	0.01259	-1.376	0.008678	-0.1971
Trial 2	0.01135	-1.216	0.007721	-0.1773
Trial 3	0.01267	-1.197	0.007706	-0.1609

Table 3.10: Generated constants for the four cases with a plate. Yet again, variations can be observed, even within the same case.

1_p	a	b	c	d
Trial 1	0.009157	-1.949	0.01041	-0.271
Trial 2	0.008023	-2.085	0.01111	-0.3105
Trial 3	0.009875	-1.797	0.0102	-0.2688
2_p	a	b	c	d
Trial 1	0.00982	-1.134	0.009675	-0.1864
Trial 2	0.008124	-1.716	0.01254	-0.2626
Trial 3	0.008512	-1.233	0.01085	-0.2277
3_p	a	b	c	d
Trial 1	0.01184	-1.844	0.007586	-0.2562
Trial 2	0.01225	-1.781	0.007547	-0.2615
Trial 3	0.008524	-2.908	0.01155	-0.6109
4_p	a	b	c	d
Trial 1	0.01139	-1.312	0.008041	-0.1876
Trial 2	0.01044	-1.496	0.009224	-0.2325
Trial 3	0.01177	-1.372	0.008215	-0.1969

From table (3.9) the follow damping model has been proposed for oscillations in water by averaging all constants except from the most deviating trial

$$y = 0.01036e^{-1.458t} + 0.0092e^{-0.2082t} \quad (3.5)$$

For oscillations in water with a plate (table 3.10) the following equation of decay is proposed

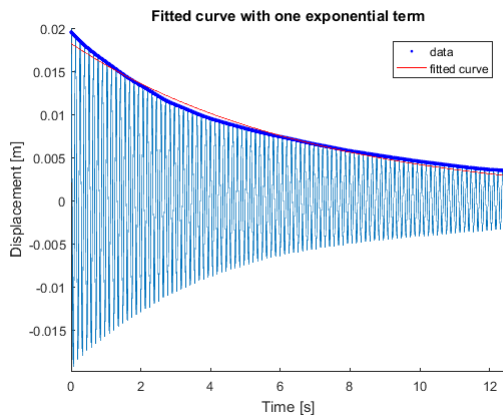
$$y = 0.01011e^{-1.6114t} + 0.0096e^{-0.1995t} \quad (3.6)$$

3.7.5 Decay in air

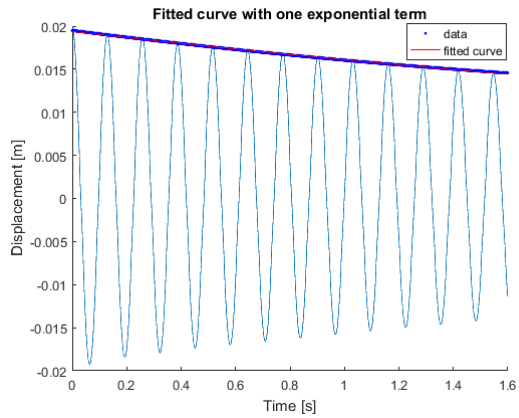
As a short comparison to the decay in water, 2_a is here presented to investigate differences in damping between air and water.

A plot of the envelope and a fitted exponential curve shows that an exponential function with one term can be used to model the damping of the system (fig. 3.26a) and an even better fit can be generated for the first 1.6 seconds (fig. 3.26b). The constants for the exponential function for the first 1.6 seconds are presented below:

$$a = 0.01937 \text{ m} \quad b = -0.1851 \text{ s}^{-1} \quad (3.7)$$



(a) A one term exponential fit can be used to give an estimate of the decay of the displacement.



(b) For the first 1.6 seconds an even better fit can be achieved with an exponential fit.

Figure 3.26: (a) depicts the envelope and a fitted one term exponential function and (b) depicts a one term fitted exponential function for the first 1.6 seconds of the motion.

Values for the 10 first peaks for a 2_w experiment (fig: 3.27), not including the starting displacement, were observed and presented in table (3.11). The first peak was not included as it may have been affected by disturbances when the motion was initialized.

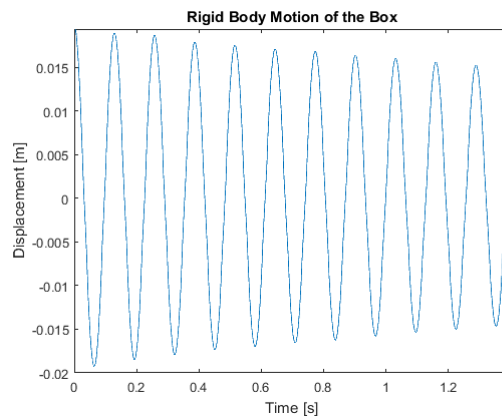


Figure 3.27: The displacement for the first 10 peaks.

Table 3.11: The peak amplitudes of the displacement not including the starting displacement. Note how the difference between two successive peaks may vary.

Displacement (mm)	18.98	18.70	17.91	17.60	17.13	16.86	16.43	16.05	15.60	15.26
-------------------	-------	-------	-------	-------	-------	-------	-------	-------	-------	-------

The displacement peaks were used to calculate the damping ratio. The damping ratio was calculated for every second peak due to the values for two successive peaks being too similar.

Table 3.12: Damping ratios calculated between every second value, starting with 18.98 and 17.91.

ζ	0.0046	0.0035	0.0033	0.0041
---------	--------	--------	--------	--------

By comparing the damping ratio for air and water in the selected time span, it can be observed that experiments in water experiences a larger amount of damping.

3.8 Discussion

From the data seen in the added mass tables it is evident that added mass increases with the addition of the plate. The addition of the plate blocks the previous path of the displaced water forcing it to change direction. This effect causes an increase of inertia in the system which is interpreted as added mass.

Although an increase in added mass does occur the overall results are similar whether the plate is in place or not. The difference is that the additional added mass does result in a slightly lower frequency. It was noted in (5.4) that the increase in added mass was between 5 and 3 %. This behavior can be seen across all measurements and it is clear that it represents the change in added mass for this particular setup. A setup with a different distance to the plate and with a different geometry of the oscillating object would experience a different fluid-structure interaction, resulting in a different added mass.

Table (3.3) illustrates that the deviation in frequency between trials is low. Therefore, comparisons between cases can be made even though the amount of trials is low.

In table (3.5) it can be seen that the added mass is larger for the stiffer and larger springs. Added mass is therefore likely related to choice of springs. The stiffer springs are larger which could cause more viscous effects. The distance to the frame also increases with stiffer springs which could change the results of the experiment. However added mass actually decreases when the box is further away from the frame, something that contradicts the observations made when the plate was introduced. One hypothesis is that the stiffer springs also have more stiffness in the radial and vertical direction which means that they are less susceptible to rotational modes. The ratio between the largest modes confirm that rotational modes are more prevalent in the results with weaker springs. The added mass also appears to increase slightly when the mass is increased but this is not investigated further. Another possibility is that the stiffer springs results in a higher force acting on the frame, making it oscillate and disrupts the motion of the box.

The acceleration of the box initially contains more noise when the plate is present compared to without it. This is likely due to a more chaotic flow as the plate changes the direction of the displaced water. This effect is disappearing as the signal loses amplitude indicating that the fluid structure phenomena is highly dependent on the distance to the structure.

The pressure at the bottom is of higher amplitude with the addition of the plate. This is believed to be from the impulse of the water acting on the box as the displaced water downwards has to change direction due to the plate blocking the way. The signal also contains more noise indicating a more chaotic flow.

The strain increases with the addition of the plate. This goes hand in hand with an increased pressure as an increased pressure results in higher loads on the box and higher loads cause larger strains.

The decay function in water required two terms to accurately describe the envelope of the displacement which is an indication that there are two damping phenomena. Conversely, the damping in air could more accurately be described using one exponential term. The decay rate was also higher in air than in water. For 2_w, it can be seen in table (7) that the two time constants b and d are of a different order of magnitude. This means that the two damping effects are of different nature. The term with the large time constant b will become zero quickly which means that this damping takes place in the beginning of the signal when the velocity is high and the distance to the structure is low. The second term has a much smaller time constant, thus this damping effect is dominant as amplitudes are lower and the distance to the structure becomes increasingly large. To determine the exact physical mechanisms behind the damping effects further studies have to be performed. An idea would be to increase the amplitude of the signal and see how an increased velocity affects the damping. It would also be of interest to increase the fluid structure interaction to see whether this would affect damping.

4 Modelling

To determine how accurately fluid structure interaction can be simulated a model of the experimental setup was constructed. The experiments were performed in LS-DYNA where the element formulation `mat_acoustic` is to be validated.

4.1 Model Setup in LS-Prepost

The creation of the model was made with the intent to resemble the experimental setup as closely as possible. The dimensions of the box and frame were thus the same as for the experimental setup. In an effort to speed up the simulation, only one quarter of the actual geometry was modelled (fig. 4.1). Symmetry planes were added to only model one quarter and this also prohibited the box from rotating which was beneficial as it removed all modes but the oscillation that was to be investigated. A full model was also tested to verify that the assumption of symmetry was valid.

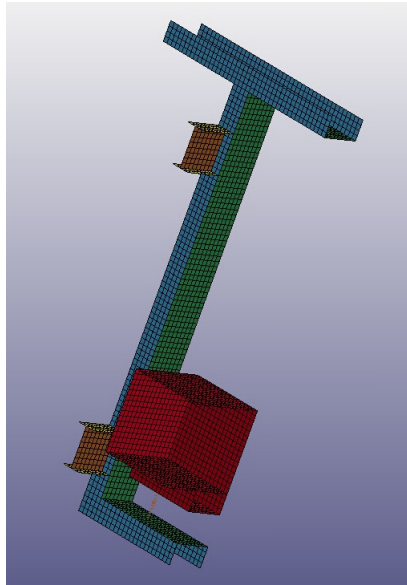


Figure 4.1: Parts with different colors have different thicknesses. The distance to the frame is different for the two different springs.

The frame and the box were constructed in Creo Parametric as shells and could be imported as 3D models. The intent was initially to import the 3D-model to LS-Prepost as a STEP-file and then mesh the model. However, meshing the frame in LS-Prepost proved to be disadvantageous and instead our supervisor helped us mesh in Hypermesh; in addition, the water was meshed in LS-Prepost. A hollow space where the box was placed was also added to the fluid part. The actual tank containing the water was modelled as a rigid boundary. Furthermore, the frame, which rests on the top of the tank in the experimental setup was locked by constraining the motion of the nodes that would have rested on the tank.

When the tetrahedral fluid mesh had been created, another issue presented itself; the fluid elements and the frame's elements did not share a boundary. This prevented the usage of the fluid-structure coupling between the fluid and the frame. The solution was to remove additional fluid sections according to figure 4.3, thus making the fluid and the structure share surfaces at the locations that were deemed necessary to include in the model. As a result, only the part of the frame beneath the box was coupled to the fluid. An additional weakness with this solution was that the "feet" of the box were filled with air rather than water hence making the box "lighter" in the simulations. Therefore, the mass of the removed water was added to the mass of the box by scaling the density. When the added mass was calculated, the extra weight from the feet was included as added mass and removed from the actual mass of the box.

The plate under the frame was modelled as rigid by cutting off part of the fluid mesh when needed (fig.4.2). The tank and the plate were locked in place with an SPC_Boundary.

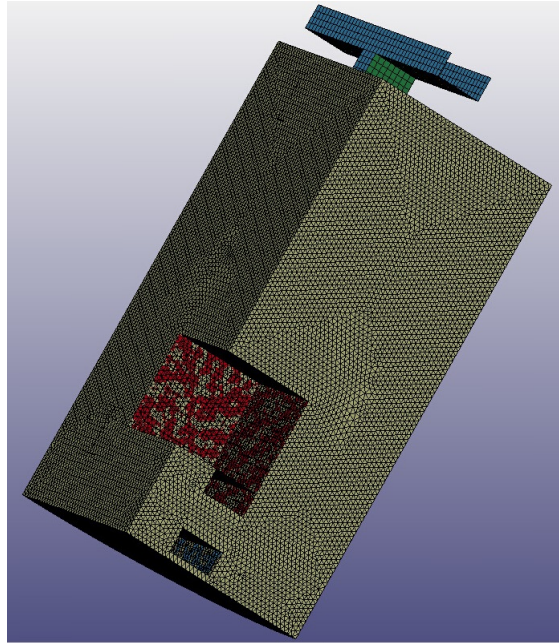


Figure 4.2: A print screen of the fluid mesh with the frame and box submerged in the fluid. In this case, the bottom part of the fluid volume is removed and the boundary represents the addition of the plate.

The experimental setups performed in water were also used in the simulations. The weight of the box was easily modified simply by changing the density of box. The stiffness of the springs were also changed in a similar manner; however, different 3D-models were needed for the two springs due to the springs not being the same length. The motion of the box was initialized by the introduction of an offset for the springs. In addition, part of the fluid volume was, as previously stated, removed to emulate the effect of the plate. All in all, two different 3D models were imported, each with the possibility to add the plate. Hence resulting in four different meshed geometries where the density of the box could be changed, adding up to eight different simulations as desired.

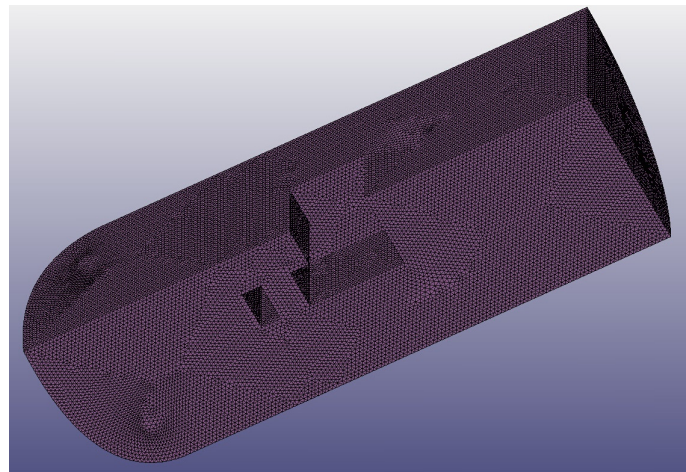


Figure 4.3: The entire fluid mesh is here presented. Note that some parts of the volume have been removed.

The coupling was added with a keyword called `Boundary_Acoustic_Coupling_Mismatch` which can be used even though the nodes do not coincide, nor do they need to be merged. In order to identify the structural surfaces that was to be coupled with the acoustic elements, a segment set had to be created. The coupling between the fluid and the structure is shown in figure (4.4). Segment set normals must point toward the fluid volume the structure is supposed to couple with.

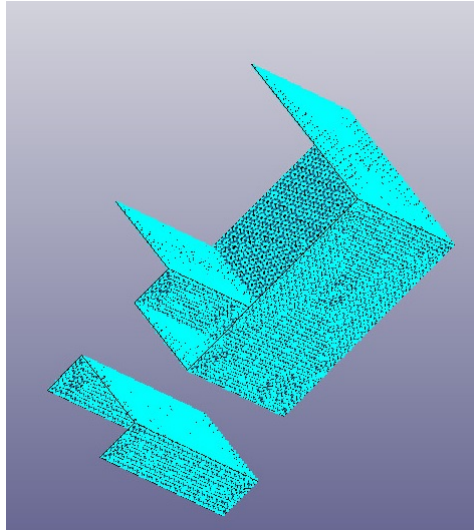


Figure 4.4: Shows the parts of the box and frame that were coupled to the fluid. However, only the side in contact with the fluid was coupled. This was controlled with the section normals.

4.2 Implemented Keywords

In this section, the different options used in the modelling in LS-DYNA are presented. The reader is referred to the appendix for the input parameters in the implemented keywords.

4.2.1 Box and Frame

The box and the frame were modelled with shell elements with the desired thickness. Element formulation 16 was used. Moreover, the material model used was Mat_Elastic. The density of the box was scaled in order to match the weight of the box in the experiments.

4.2.1.1 Element Formulation 16

Shell type 16 requires approximately 2.5 times more CPU than type 2 shells. However, the accuracy is in many cases higher. The advantage of element formulation 16 is that it uses full integration except for the transverse shear, where it uses one point integration. Therefore, it reduces hour-glassing as well as shear-locking. Moreover, element type 16 yields the correct solution for warped elements when used with hour-glass control 8 [10].

4.2.2 Acoustic Volume

The fluid elements are solid tetrahedral elements and the material model Mat_Acoustic was used together with element formulation 8.

4.2.2.1 Mat Acoustic

Mat Acoustic is a material model utilizing the single degree of freedom displacement potential formulation. Mat acoustic is appropriate for tracking low pressure stress waves in an acoustic media such as air or water. This element formulation is rather new in LS-DYNA and has the benefit of being very cost effective [7].

4.2.3 Discrete Elements

The springs were created as discrete spring elements. The stiffness of the springs corresponded to the average spring constant and was chosen in the material keyword Mat_Spring_Elastic.

4.2.4 Hourglassing and Control Keywords

In order to further increase the accuracy of the FE-model the Hourglass and Control keywords were implemented. The Hourglass keyword reduces hour-glassing and was used for the box and the frame.

The `Control_Accuracy` option is recommended for shell elements even though it has a higher cost. [7].

The `bulk_viscosity` keyword was used as it is recommended when treating shock waves. It adds a viscous term to the pressure in order to smear shock discontinuities into rapidly varying yet continuous transition regions [7]. The reader is referred to the LS-DYNA theory guide [9] for a more detailed explanation.

The `Control_Energy` keyword controls the type of energies that are to be included in the energy balance [7].

4.3 Sources of Error in Simulations

Several simplifications and assumptions were made with regards to the experimental setup. As previously mentioned, fluid mesh was removed inside the "feet" of the box. The weight of this water was accounted for by adding it to the mass of the box and this is believed to be an acceptable approximation. Not coupling other parts of the frame to the fluid except the bottom beam was believed to be acceptable as no significant fluid structure interaction should take place elsewhere. No fluid coupling was included for the tank or the plate. Instead, those surfaces were approximated as rigid surfaces resulting in reflective boundaries. An infinite water depth was assumed for the fluid in the FE-model which was supported by the convergence study on fluid volume size in section 4.7.3.

Large displacements and deformations introduce errors as the fluid structure coupling is fixed in space.

In the experiments a heavier box was achieved by filling it with water. In the model the inside of the box was instead kept empty and the heavier mass was emulated by a scaling of the density for the edges of the box. It was believed that this should not impact the motion of the box which is also confirmed by simulations for different densities. However, the dynamic response of the box's walls could be affected due the walls not having the right density and not having water on both sides. If the density is incorrect, that means the inertia of a wall oscillating is incorrect, the vibration of the walls are therefore not modelled correctly. In addition, having water on both sides would provide additional stiffness to the walls, something that is not accounted for in our model.

Another assumption that could affect the results is that viscous effects are not included in the model which is evident from the fact that the motion is not damped. The damping not only affects the amplitude but also the frequency which should be taken into consideration when interpreting the results. The change of frequency has been shown (3.7.4) to be insignificant.

The springs were modelled as discrete springs and the actual geometry of the springs was not accounted for in the FE-model.

A ratio between the mesh size and the structure size of 0.025 was chosen for the FE-model for practical reasons. The convergence study performed in section 4.7.2 showed that the frequency had not converged fully for that ratio. The specific ratio was close to convergence but minor inaccuracies could have been introduced.

4.4 Modelling Results

From the simulated model the same results as from the experiment were collected. This was done in order to have experimental data to compare the model to.

4.4.1 Displacement

The difference of the displacement is small for motions with and without an added bottom plate (4.5). At the end of the wave a small decrease in frequency can be seen when adding the plate. The period of the wave is around 0.17s.

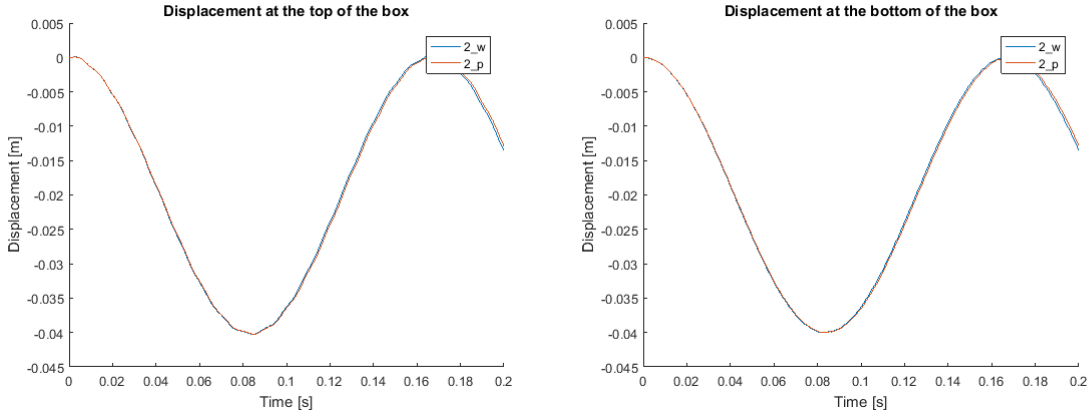
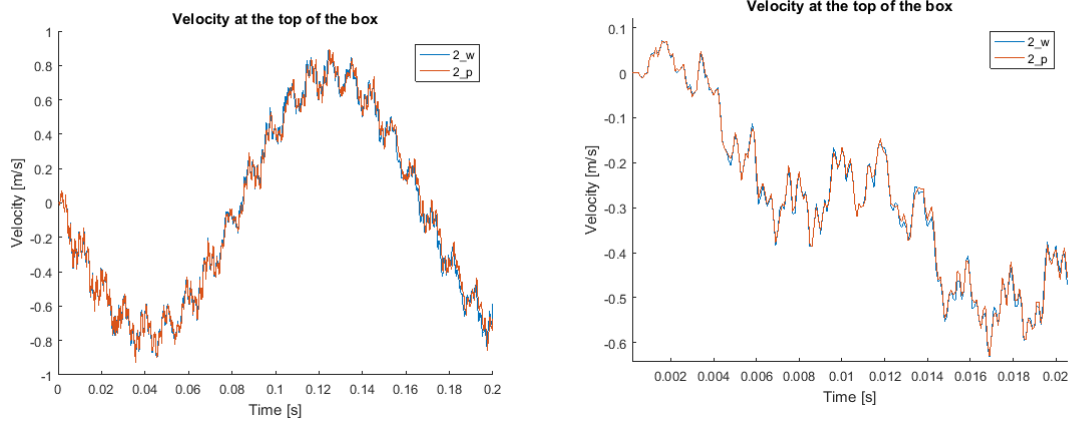


Figure 4.5: The displacement is extracted from nodes located in the center of the box at the top and the bottom, the displacement is only extracted in the same direction as the main oscillation. The amplitude is prescribed as double the offset of the springs in the model and is $0.04m$ hence the wave is oscillating around $-0.02m$.

4.4.2 Velocity

The velocity at the top of the box consists of waves of two different frequency and on top of that there is high frequency noise (fig. 4.6). The low frequency wave has a period around $0.16s$ and an amplitude of $0.8m/s$. On top of the low frequency wave, a wave of low amplitude and of a higher frequency can be seen. That wave has a period of around $0.01s$ and an amplitude of around $0.1m/s$. The addition of the plate does not seem to have any clear influence on the velocity.

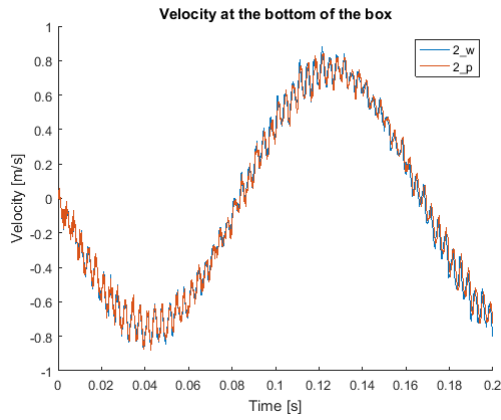


(a) The velocity measurement consists of a large sinusoidal wave of a period around $0.16s$ and an amplitude of $0.8m/s$

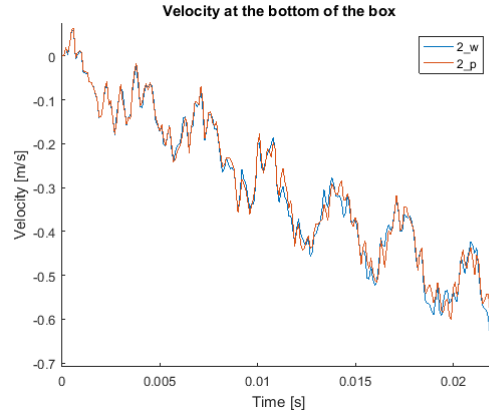
(b) On top of the large wave a smaller wave of a higher frequency can be seen. That wave has a period of around $0.009s$ and an amplitude of around $0.1m/s$

Figure 4.6: The velocity at the top is extracted from a node in the middle of the bottom of the box. The presented velocity is the velocity in the same direction as the main oscillation.

The velocity at the bottom consists of waves of two different frequency and on top of that there is high frequency noise (fig. 4.7). The low frequency wave has a period around $0.16s$ and an amplitude of $0.8m/s$. On top of the low frequency wave, a wave of low amplitude and of a higher frequency can be seen. The wave has a period of around $0.003s$ and an amplitude of around $0.1m/s$. The addition of the plate does not seem to have any clear influence on the velocity at the bottom.



(a) The velocity measurement consists of a large sinusoidal wave of a period around 0.16s and a amplitude of 0.8m/s.



(b) On top of the large wave a smaller wave of a higher frequency can be seen. That wave has a period of around 0.0033s and an amplitude of around 0.1m/s.

Figure 4.7: The velocity at the bottom is extracted from a node in the middle of the bottom of the box. The presented velocity is the velocity in the same direction as the main oscillation.

4.4.3 Acceleration

The acceleration at the top changes values from -1000 m/s^2 to 1000 m/s^2 in milliseconds. The acceleration is similar with or without a plate (fig. 5.3).

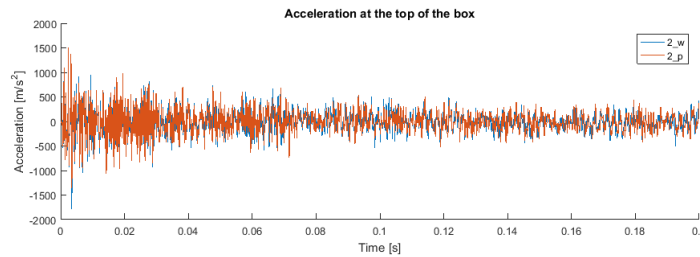


Figure 4.8: The acceleration is seemingly randomly varying around zero although initially decreasing in value. The acceleration can alter between very high positive and negative values in a short amount of time.

The acceleration at the bottom of the box changes values from -1000 m/s^2 to 1000 m/s^2 in milliseconds. The acceleration is similar with or without a plate (4.11b).

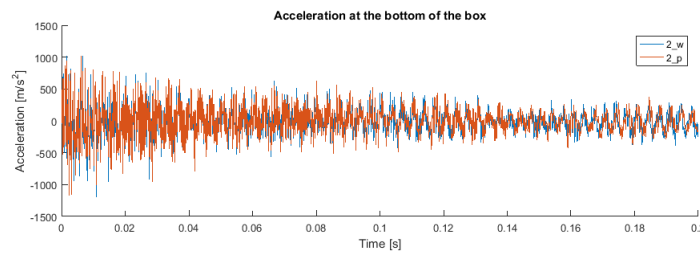
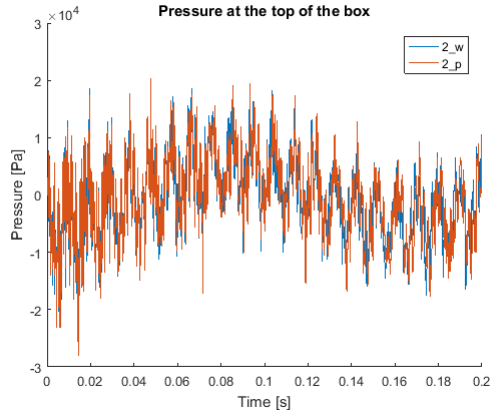


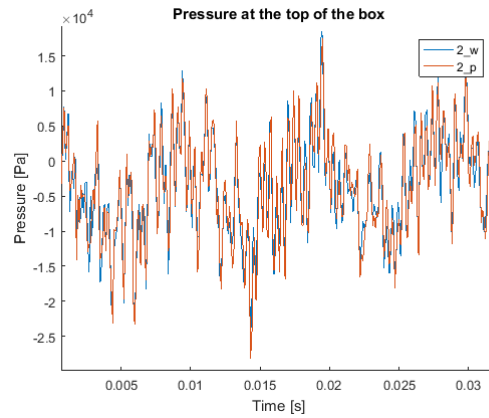
Figure 4.9: The acceleration is seemingly randomly varying around zero although initially decreasing in value. It alternates between very high positive and negative values in a short amount of time.

4.4.4 Pressure

The pressure at the top of the box consists of a low frequency sinusoidal wave with a period of around 0.16s and an amplitude of roughly $8kPa$ (fig. 4.10). Around this low frequency wave there is a wave of a higher frequency. The high frequency wave has an amplitude of $5kPa$ and a period of 0.01s. It is a signal with high frequency noise it which can be seen in the zoomed in image below.



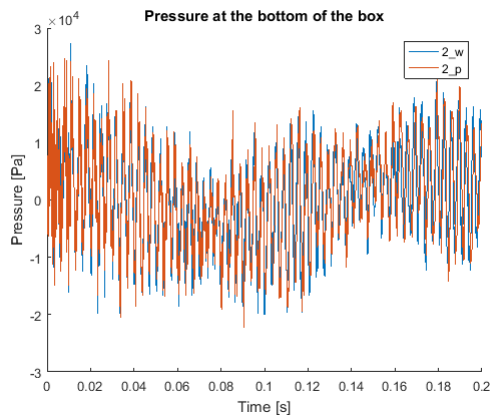
(a) The pressure consists of a larger sinusoidal wave with a period of around 0.16s. Around this large sinusoidal wave there is a wave of a higher frequency.



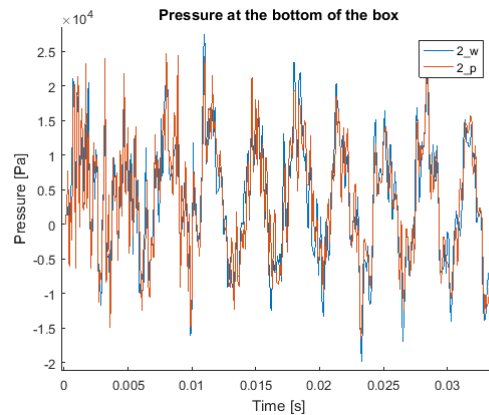
(b) The high frequency wave is a signal with an amplitude of $5kPa$. The high frequency wave is full of noise of an even higher frequency.

Figure 4.10: The pressure is measured at the first of seven integration points of a solid element located above the top center of the box.

The pressure at the bottom of the box consists of a low frequency sinusoidal wave with a period of around 0.16s and an amplitude of roughly $5kPa$ (fig. 4.11). Around this large sinusoidal wave there is a wave of a higher frequency with an amplitude of $10kPa$ and a period of 0.003s.



(a) The pressure consists of a larger sinusoidal wave with a period of around 0.16s. Around this large sinusoidal wave there is a wave of a higher frequency.



(b) The high frequency wave is a signal with an amplitude of $10kPa$ and a period of 0.003s. There is noise in the signal.

Figure 4.11: The pressure is measured at the first of seven integration points of a solid element located beneath the bottom center of the box.

Fringe plots of the pressure in the water are presented below in order to compare with the experiments. The first three figure (4.15, 4.16 and 4.17) are three consecutive data dumps of the pressure while the box is travelling upwards. The data dumps are $4ms$ apart in time. Here it can be seen that there is a higher pressure in the direction of the box's velocity and also in an area between the frame and the box. There are areas of low pressure present beneath the box. Furthermore it is noted that there are occurrences of large pressure changes from one figure to the next, especially from figure (4.16) to figure (4.17) where an area of high pressure between the box and the frame disappears.

The following three figures (4.12, 4.13 and 4.14) are images of when the box is travelling downwards. Here there is a high pressure zone in the direction of the bow's motion in the first image (fig. ref1down) and areas of low pressure above the box in the two following images (fig. 4.13 & 4.14). The most notable change here is that between figure (4.13) and (4.14) a zone of high pressure beneath the box disappears in the following images. It should be noted that the time between the data dumps is much longer than the time step used in the calculations. The red grid in the figures is the box which is made transparent.

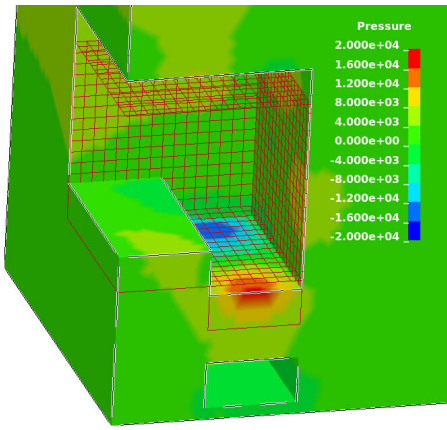


Figure 4.12: The image is taken at $t=0.16968$

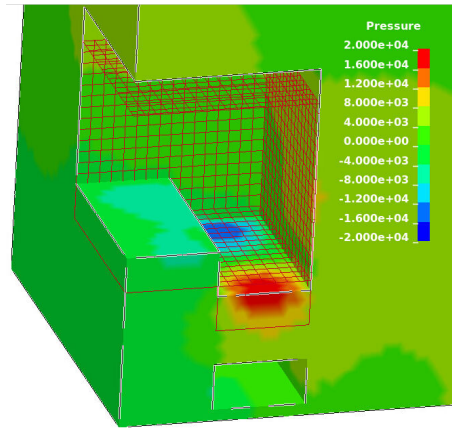


Figure 4.13: The image is taken at $t=0.17371$

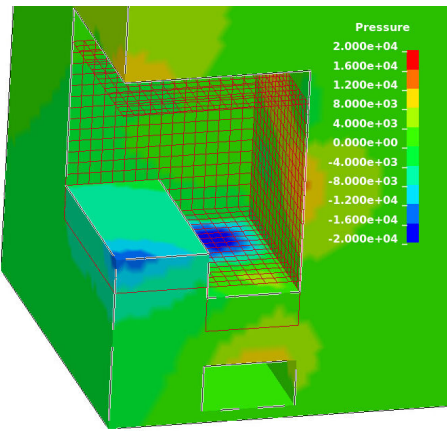


Figure 4.14: The image is taken at $t=0.17776$

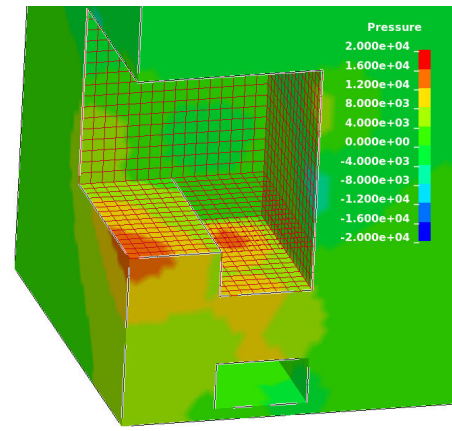


Figure 4.15: The image is taken at $t=0.08887$

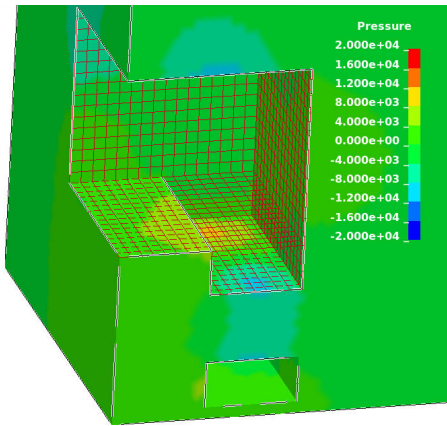


Figure 4.16: The image is taken at $t=0.09291$

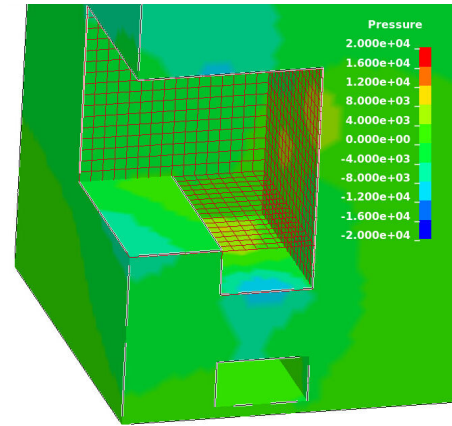


Figure 4.17: The image is taken at $t=0.09695$

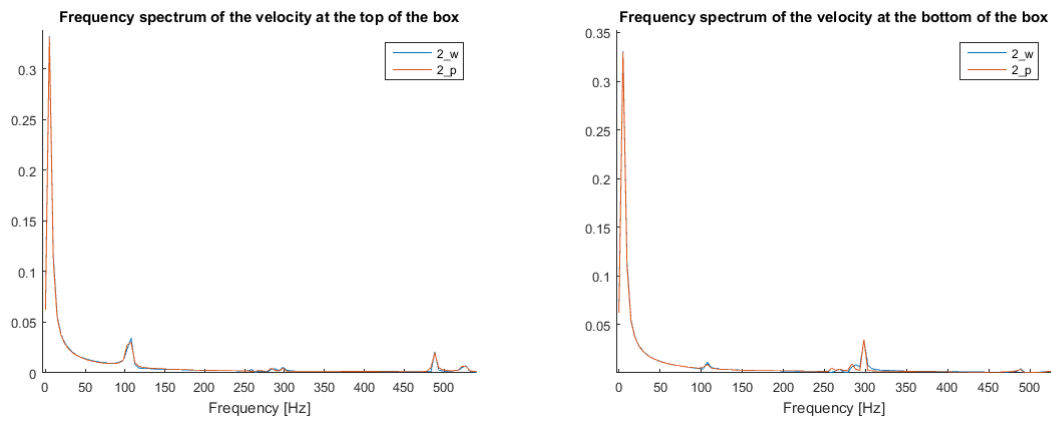
4.5 Frequency Domain and Filtering

It is evident from the previous section that the generated data from LS-DYNA contain signals of different frequencies. Spectrograms for a fast Fourier transform of the different signals are used to illustrate the different frequencies contained in a signal (4.18).

4.5.1 Velocity

At the top of the box frequency peaks can be observed at both 5 and 100 Hz. Some smaller peaks at higher frequencies can also be observed. At the bottom of the box there is a large peak at 5 Hz

and a smaller peak at 300 Hz. With and without plate have similar spectra for both the top and the bottom.



(a) A larger frequency peak can be observed at roughly 5 Hz and smaller peaks at 100 and 500 Hz. 2_w and 2_p have similar spectra.

(b) A large peak at 5 Hz and a smaller peaks at 300 Hz can be observed. 2_w and 2_p have similar spectra.

Figure 4.18: Both graphs have similar peaks at 5 Hz but a much larger peak is observed at 100 Hz for the top whilst a larger peak can be observed at 300 Hz for the bottom velocity (4.18a)

It appears the top and bottom share the first mode and then have different natural frequencies for higher modes.

4.5.2 Acceleration

The acceleration at the top of the box contains several peaks as can be seen in figure (4.20). The frequency peaks with and without the plate coincide. It is evident that the lower frequencies are covered in high frequency noise.

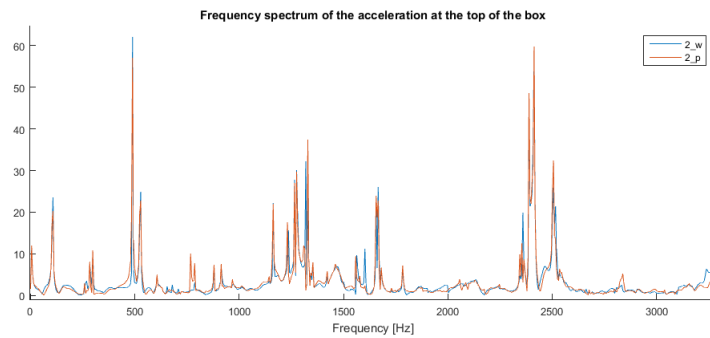


Figure 4.19: The frequency spectrum for 2_w and 2_p. The spectrum coincides well for the two cases. Peaks can be seen at 5, 100, 300 and 500 Hz as well as noise at high frequencies.

The acceleration at the bottom of the box also has a small peak at 5 Hz but also a large peak at 300 Hz. Like the top acceleration the bottom acceleration contains several peaks of higher frequency.

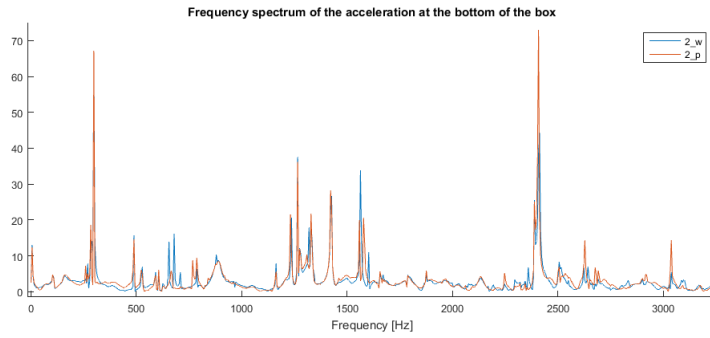
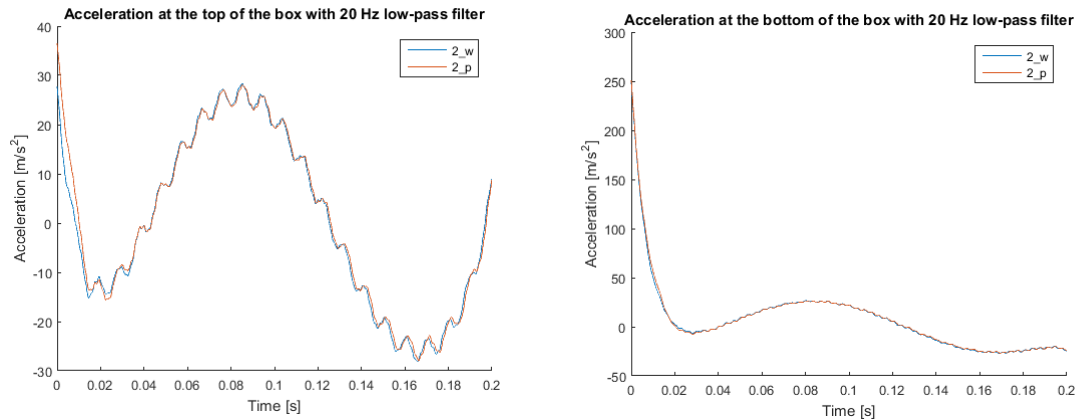


Figure 4.20: The frequency spectrum for 2_w and 2_p. The spectrum coincides well for the two cases. A small peak at 5 Hz and a large peak at 300 Hz is observed. The figure also illustrates noise at high frequencies.

To extract a low frequency acceleration, a 20 Hz low-pass filter was used. The filter produces a signal of roughly $30m/s^2$ in amplitude and around $6Hz$ in frequency at both the top and the bottom. Some filter artifacts can be seen in the figures due to the choice of filter.



(a) A filter of the first order was used which is why traces of higher frequencies than 20 Hz are present.

(b) After 0.02s the filtered wave becomes sinusoidal.

Figure 4.21: The filtered signals are sinusoidal except in the beginning and the end. Some artifacts can be seen.

4.5.3 Pressure

The pressure at the top contains peaks at 5, 100, 300 and 500 Hz (4.22). There are also peaks at higher frequencies which are not regarded. The pressures were extracted from fluid element next to the center of the box.

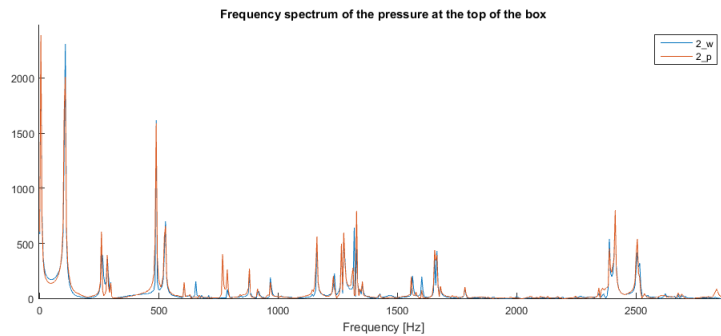


Figure 4.22: The frequency spectrum for 2_w and 2_p. The spectrum coincides well for the two cases. Peaks can be seen at 5, 100, 300 and 500 Hz as well as noise at high frequencies.

At the bottom of the box the pressure peaks at 5, 100 and 300 Hz (4.23).

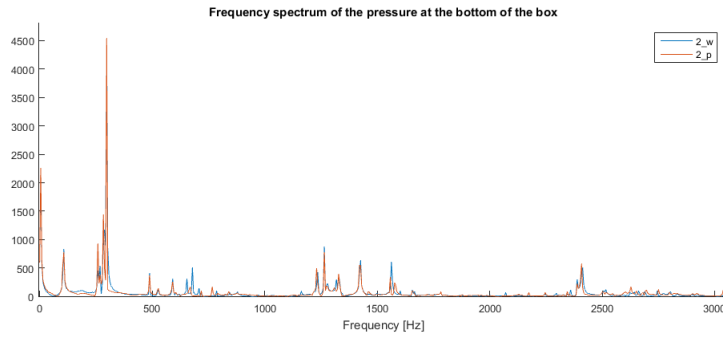
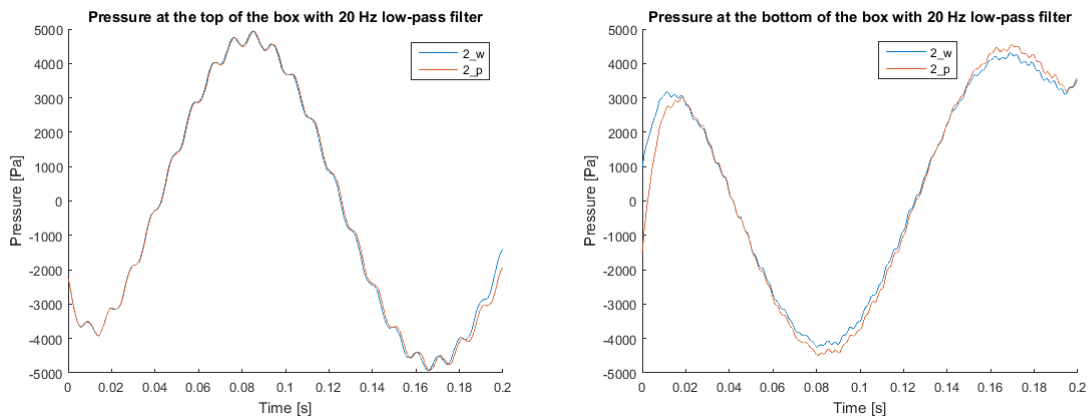


Figure 4.23: The frequency spectrum for 2_w and 2_p. The spectrum coincides well for the two cases. Peaks can be seen at 5, 100, and 300 Hz.

The pressure was filtered using a first order low pass filter to extract the pressure variation of low frequency. Here it can be seen that the sinusoidal pressure at the bottom and the top are separated in phase by π . The pressure at the top and bottom are both roughly $4500 Pa$.



(a) The pressure with and without the plate coincide.

(b) The pressure is slightly higher with the plate.

Figure 4.24: The filtered pressure is in the order of magnitude of kPa . Some artifacts from the filtering can be seen.

From the pressure it can be concluded that the box is travelling downwards as the pressure is negative at the top and positive at the bottom. This is indeed the case. Furthermore, the pressure for 2_w and 2_p are more coincident at the top than the bottom; the pressure for 2_p is higher than for 2_w in figure (4.24b). Moreover, the pressure in figure (4.24a) has a second shorter frequency.

4.6 Added Mass Simulations

The frequencies and corresponding added masses for the simulations are presented in table (4.1).

Table 4.1: The simulated results without the plate are presented in the left table and the results with the plate in the right table. The added mass is higher when the plate is present.

	f [Hz]	m_a [kg]
1_w	6.99	48.4
2_w	5.99	48.4
3_w	9.42	48.4
4_w	8.07	48.5

	f [Hz]	m_a [kg]
1_p	6.94	49.6
2_p	5.96	49.5
3_p	9.37	49.2
4_p	8.04	49.4

As evident from table (4.1), the added mass remains constant for 1_w-4_w. On the other hand, the added mass decreases slightly for 3_p-4_p compared to 1_p-2_p.

An increase in added mass can be observed when comparing simulations with and without the plate. The added mass for the simulations with the plate is roughly 2 % larger than without the plate.

The added mass in the simulations is 48-49 kg:s but how does it compare to the analytical added mass? Without the plate, the analytical added mass is 4 % larger than the simulated added mass. For the simulations with a plate, the same number is 1-2%. Keep in mind that the analytical solution does not account for the effect of the plate.

4.7 Convergence studies

4.7.1 Fluid Mesh Size for Solid Elements

As the majority of elements in the model are fluid elements the mesh sizing of the fluid elements is of great importance in regards to decrease the computational time. Simulations with a simplified model were conducted in order to determine the effect of using different element sizes. The simplified model is a box submerged in a cubic fluid volume which is oscillating due to 4 initially offset springs. In the model the box was locked in horizontal displacement along the edges. The model can be seen below (fig. 4.25).

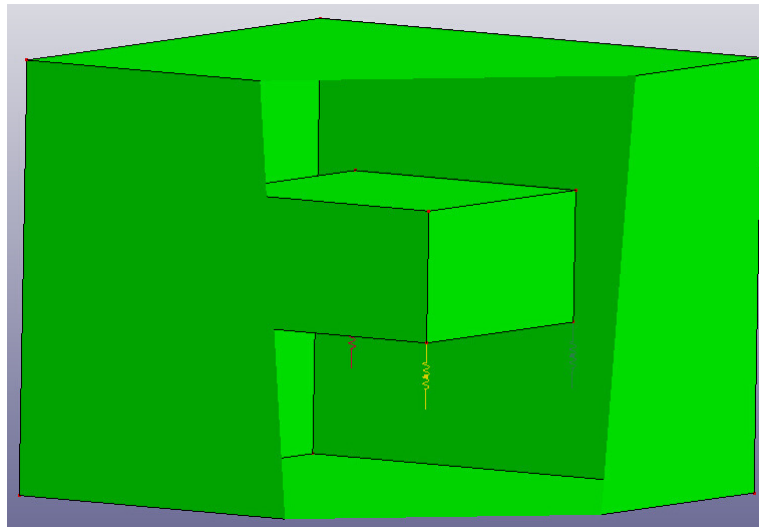


Figure 4.25: The simplified model is used to explore the mechanics behind acoustic fluid elements. The box is $0.2 \times 0.2 \times 0.1$ in size and the water volume is $0.4 \times 0.4 \times 0.33$. The box is solid and centered inside the fluid.

The simulations used different sizes of the fluid elements and as a consequence the frequency changed, the results can be seen below (fig. 4.26).

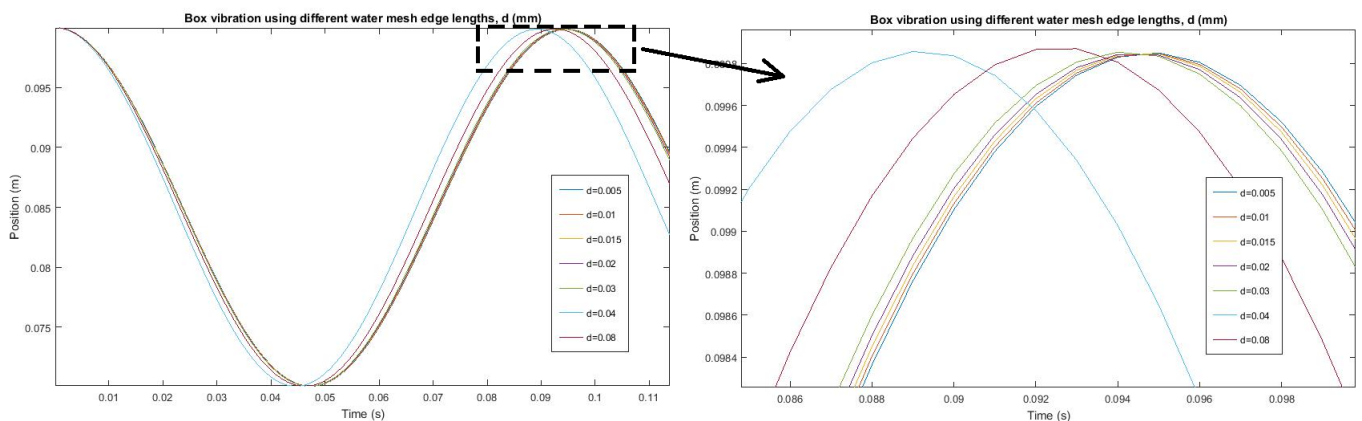


Figure 4.26: The results are from the same LS-DYNA model where everything is equal apart from the side length of the fluid mesh. It can clearly be seen that the frequency decreases with larger fluid elements. See the previous image for the geometry of the model.

As can be seen in the figure above, the period decreases with a increase in fluid element size. However when the fluid elements become very large, $d = 0.08mm$ the period increases compared

to the second largest size $d = 0.04$. This could be from a general inaccuracy when using large fluid elements. Simulations were also conducted using elements of larger sizes than $8mm$ but those wouldn't work due to a lack of contact nodes between the fluid and the structure.

Table 4.2: The structure side length is $0.2m$. The frequencies are presented for the fluid mesh side length and a dimensionless parameter defined in the table. The frequency converges at the dimensionless number 0.075.

Fluid mesh side length (m)	0.005	0.01	0.015	0.02	0.03	0.04	0.08
Fluid mesh side length/structure side length	0.025	0.050	0.075	0.100	0.150	0.200	0.400
Frequency (Hz)	10.55	10.55	10.55	10.58	10.62	11.22	10.81

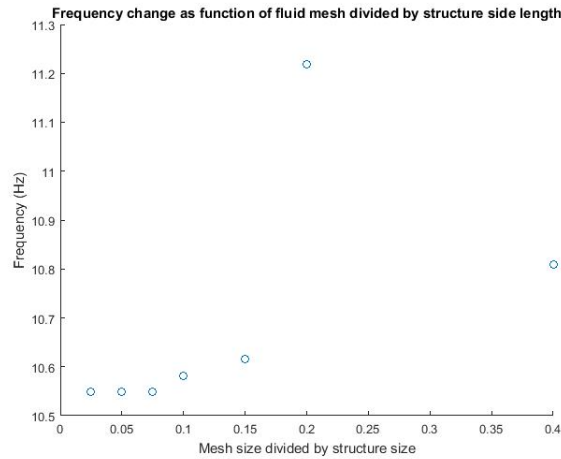


Figure 4.27: The data from the scatter plot suggests that the characteristic length for the fluid mesh should be kept smaller than 7% of the characteristic length of the structure surface.

4.7.2 Fluid Mesh Size for Shell Elements

The modelling of a structure can also be performed with shell elements and a convergence study for such a case is here presented. The study was performed similarly to how the study for solid elements was performed and the motion of the box for the different element sizes are presented in fig. (4.28). To get a more accurate frequency, some of the data had to be fitted as a Fourier series. Graphs with poor resolution have not been fitted with a Fourier series. The keyword `Control_Bulk_Viscosity` was also included in the mesh study for the shell elements. The different mesh sizes are referred to as their dimensionless quantities unless otherwise stated (table 4.3). Note that the box was locked in horizontal displacement along the edges.

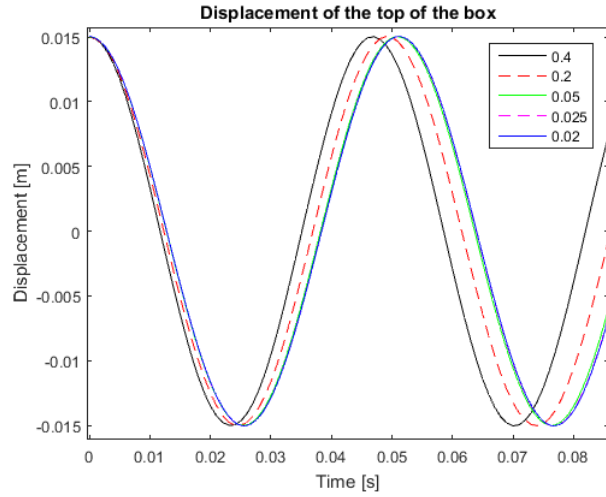


Figure 4.28: The displacement of the top of the box for the different tests. The frequency decreases and 0.05, 0.025 and 0.02 yield plots that are of similar frequency. 0.05 became unstable after the plotted time interval.

It was found for some cases that the structure started to deform and oscillate in ways that were not expected and were therefore not included in figure (4.28). All cases and their corresponding frequencies are presented in table (4.3). The simulation with an element side length of 0.01m did not start deforming until after one wavelength and was therefore included in figure (4.28) even though it was not stable for the entire simulation. The entire motion for element size 0.01m can be seen in figure (4.29)

Table 4.3: The structure side length is 0.2m. The results are presented for the mesh side length and the dimensionless number. The symbol – means that the structure started to deform unexpectedly. 0.05 did deform but the deformation did not start until after a full wavelength. The simulation has not fully converged at 0.02.

Fluid mesh side length (m)	0.004	0.005	0.01	0.015	0.02	0.04	0.08
Fluid mesh side length/structure side length	0.02	0.025	0.05	0.075	0.1	0.2	0.4
Frequency (Hz)	19.53	19.55	19.65	-	-	20.33	21.36

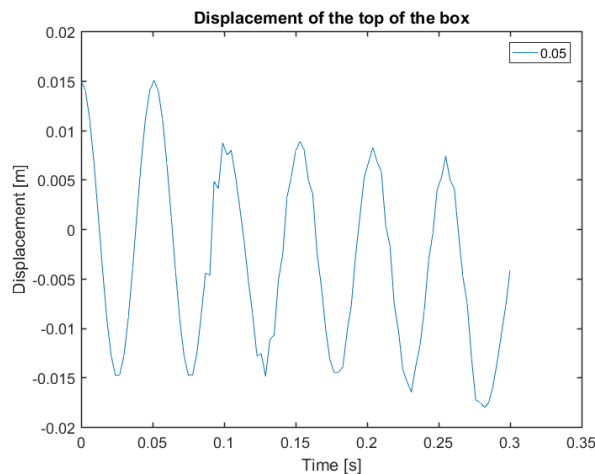


Figure 4.29: The model appears to be stable one and a half wavelength but then breaks down. The resolution of the motion is unfortunately quite poor but it is linked to the amount of times the results were updated and not the actual displacement of the model.

Figure (4.28) illustrates that the displacements for 0.025, 0.02 and 0.05 are close and table (4.3) reveals that the frequency is converging but not yet fully. It is important to keep in mind that

0.05 was only reliable for the time presented in figure (4.28). Another interesting observation was that the simulation was stable for 0.2 and 0.4 even though the simulation for 0.1 was not.

Illustrated in figure (4.30) is the deformation of the box for a failed simulation, in this case for 0.015 m in element size. From left to right the images shows the structure at $t=0.021$, 0.024 and 0.027 seconds.

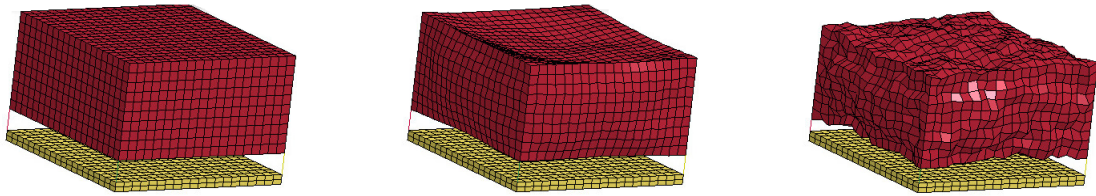


Figure 4.30: 0.015 m in element size makes the simulation unstable causing the following deformations as time progresses.

In figure (4.31) a fringe plot of the pressure right before the deformation illustrates how pressure peaks are generated in a pattern next to the box's walls. It should also be noted that the values of the peaks are much higher than the pressure for cases where no deformation occurs.

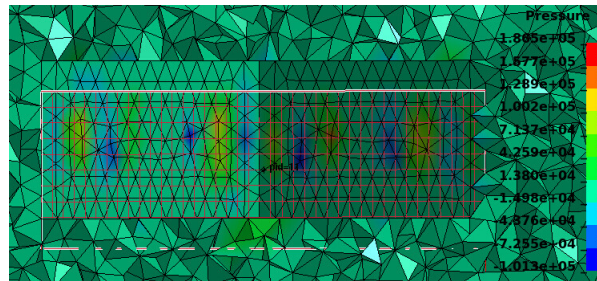


Figure 4.31: Pressure zones alternate between high and low pressure in a regular pattern. The pressure is also higher than for stable simulations.

To investigate whether an increase of stiffness would stop the model from deforming Young's modulus was increased 10 times. Figure (4.32) illustrates the motion for the element size 0.02 m after the structure has been made stiffer. The resolution is once again quite poor but it can be observed that the frequency for the higher E-modulus is the same as for the lower E-modulus until the lower E-modulus breaks down. It can also be seen from the figure that the model with the higher stiffness remains stable.

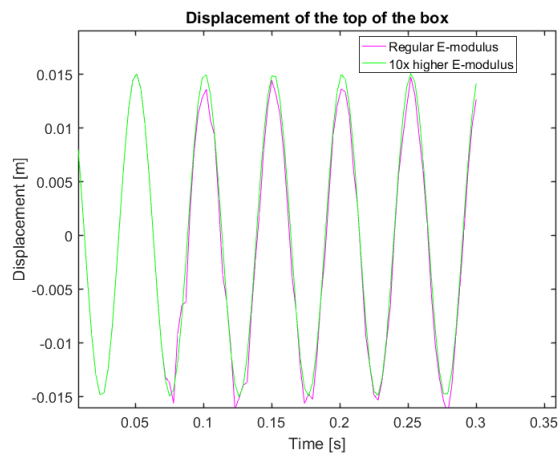


Figure 4.32: The model with the higher E-modulus is more stable than the same model with a lower stiffness. It should also be noted that the frequency is the same.

Finally, the ratio between the element side length and the characteristic length was plotted versus the corresponding frequency (fig. 4.33).

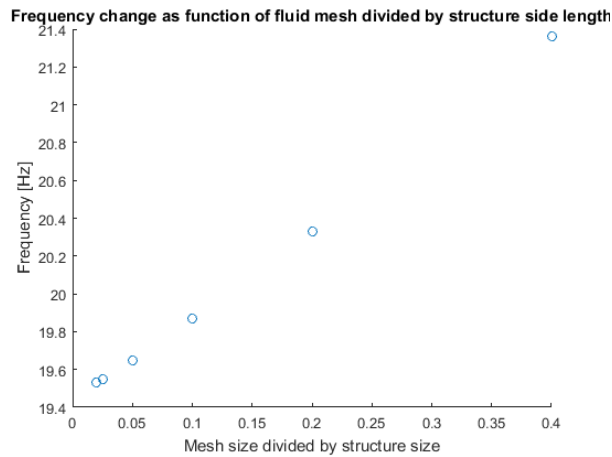


Figure 4.33: The graph suggests a linear condition between frequency and mesh size.

From figure (4.33), it can be seen that the frequency decreases linearly with the element size. Moreover it shows that the results have not converged yet. The frequency for the lowest ratios are however of similar value.

4.7.3 Fluid Volume

How large fluid volume is required in order to assume infinite fluid depth? Simulations with a simplified model (fig. 4.34) were conducted in order to determine the required fluid volume in order for the vibration characteristics to remain constant to a small change of fluid volume. The box was a solid modelled using elastic solid elements. The box was locked in horizontal displacement along the edges.

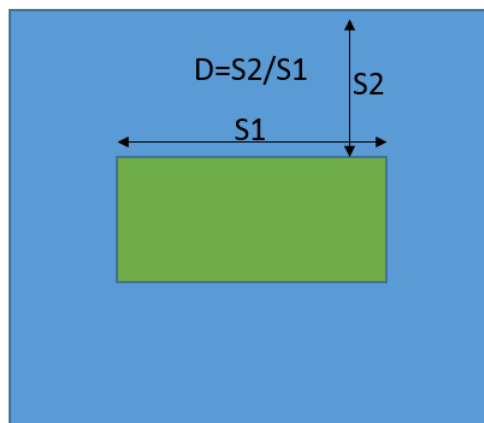


Figure 4.34: The same model used in the fluid mesh size experiments was used. However this time the fluid mesh size remained constant and the fluid volume was changed instead.

In fig. (4.35) it can be seen that frequency decreases with D . After D reaches 1.4 infinite water fluid depth is reached as an increment in D does not change the frequency. This can be seen as $D = 1.4$ and $D = 2.225$ coincide.

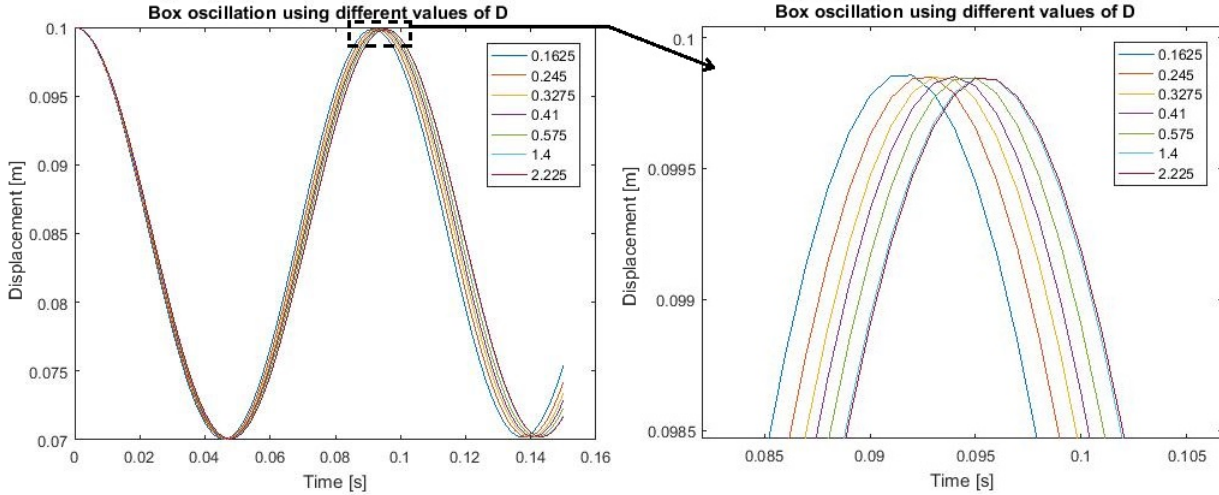


Figure 4.35: The same model used in the fluid mesh size experiments was used. However this time the fluid mesh size remained constant and the fluid volume was changed instead.

4.8 Discussion

Table (4.1) show that the added mass is roughly the same for the different cases. In other words, the stiffness of the springs and the mass of the object has no effect on added mass, only a small difference in added mass can be seen for simulations with a plate. This is likely due to a change of distance to the plate which occurs when springs are changed.

A comparison between the added masses in table (4.1) reveals that the added mass increased when the plate was introduced. A theory as to why the added mass increases is that the introduction of a rigid boundary reflects pressure waves on to the box resulting in an increase of inertia.

From comparing figure (4.6) and (4.7), one can see that the frequencies of the high frequent waves seen in the velocity and the pressure for the top and bottom are different. It turns out the frequency of the high frequent waves calculated at the bottom is higher than at the top. The high frequent waves are believed to be vibrations in the sides of the box. This implies that the stiffness of the lid is lower than the stiffness of the bottom part, as natural frequency increases with stiffness. This is intuitive since the feet at the bottom of the box help stiffen that area, making it less susceptible to bending.

From the fringe plots of the fluid pressure it is clear that large pressure differences occur in short amounts of time. This is due to the acoustic modelling of the pressure where transient pressure waves propagate through the fluid at 1500 m/s^2 . The pressure at the bottom boundary in the fluid is low indicating that the addition of the plate is of low significance in the FE-model. In figure (4.16) high and low pressure can be seen in the region between the box and frame below. This indicates that the interaction in this area dominates as a source of fluid structure interaction compared to the bottom plate.

Three different convergence studies were performed for Mat_Acoustic. The study regarding mesh size when the structure was modelled as a solid yielded a ratio of 0.075 between the element side length and structure side length for the frequencies to convergence.

The study for infinite water depth for the solid structure yielded a ratio of 1.4 between the structure side length and the distance to any outer fluid boundary. Fluid elements modelled further away than this distance have no effect on the results of the model if the boundaries are not rigid.

For certain shell elements sizes the structure was deformed and subjected to unreasonably high pressures. Interestingly, these stability issues occurred with both small and large element sizes, leading to the conclusion that smaller element sizes are not necessarily more stable. The unexpected deformation is believed to be due to Mat_Acoustic not handling deformations in the material well since a higher value for Young's modulus decreased the deformation. After decreasing the mesh size to 2.5 % of the structure length and beyond, only a small change in frequency could be observed. Choosing values below 2.5 % becomes a trade off between accuracy and computational cost.

5 Comparison between Experiment and Simulation

5.1 Displacement

A plot of the displacement from the experiment and the simulation is here presented to better visualize the motion for the different cases (fig. 5.1).

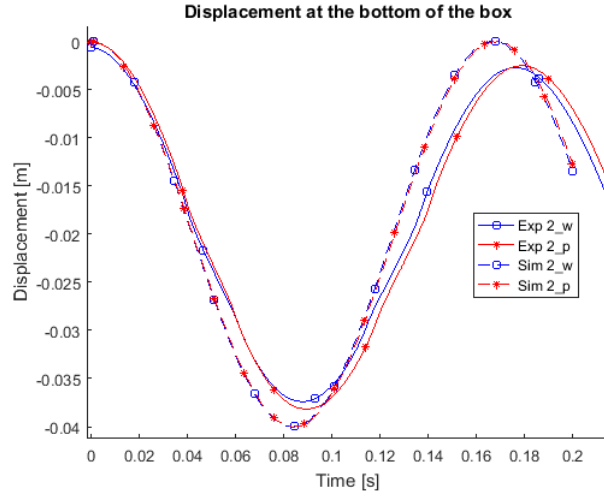


Figure 5.1: The experimental wave is not a perfect sine due to the influence of rotational modes.

From figure (5.1), a few observations can be made. Firstly, only the experiments are affected by damping which can be seen as the wave propagates. Secondly, it is clear that the frequency for the simulations are higher than for the experiments. Lastly, the plate decreases the frequency for both the experiments and the simulations.

5.2 Acceleration

To compare the acceleration between the model and the experiment new data of the acceleration from the model was derived from the displacement. From considering the displacement to be a harmonic wave.

$$y = A\cos(\omega t) + B \quad (5.1)$$

The acceleration was derived to be

$$y'' = -A\omega^2 \cos(\omega t) \quad (5.2)$$

By the assessment of the acceleration from the model the values between the model and the simulation can now be compared.

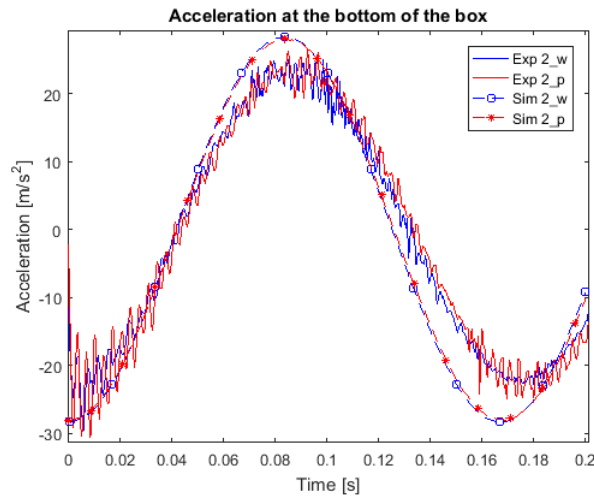


Figure 5.2: For both the simulation and the experiment there is no significant change in the acceleration when the plate is added.

As can be seen in fig (5.2) the acceleration is larger in the model. However this could be a consequence of frequency not being constant in the comparison. To investigate this further the simulated acceleration is adjusted in both frequency and amplitude to the ratio of f_{exp}/f_{sim} . From (eq. 5.2) it follows that for a change in frequency the amplitude should be adjusted by the square of the ratio.

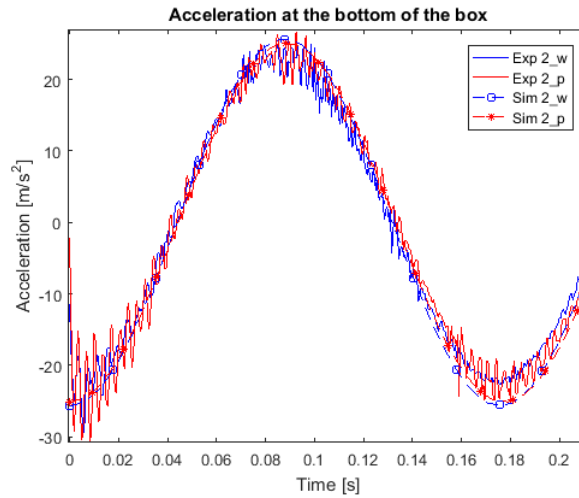


Figure 5.3: The simulated acceleration is here adjusted to the frequency of the experimental acceleration. Note that the decay is not considered in the case of the simulation.

5.3 Pressure

From analyzing the fringe plots presented in 4.4.4 one can conclude that the pressure in the model is very different from the pressure in the experiments. The pressure measured in the experiments resemble a harmonic wave (fig.3.15) whereas the pressure in the model can change dramatically from high to low in milliseconds. In the experiment the highest pressure is measured to be around $10kPa$. In the model the pressure can be higher where values of $20kPa$ and above have been noted. A filtered pressure signal is presented in section 4.5.3

5.4 Summation of Results

The frequencies for all different cases were calculated from the displacement and are presented in table (5.1) on the next page. The added masses correspond to the previous frequency in the table. At a first glance it can be concluded that the model underestimates added mass by around $9kg$ or 15% . The added mass in the experiments is roughly $60kg$ and in the model it is roughly $50kg$. As the plate is introduced added mass increases in the experiment by $2kg$. In the model it increases by $1kg$.

Table 5.1: The results of the experiments averaged into single values are presented here.

Lc	k_{Total} [kN/m]	m_{Box} [kg]	$f_{Analytic}$ [Hz]	m_{Added} [kg]	$f_{Measured}$ [Hz]	m_{Added} [kg]	$f_{Simulated}$ [Hz]	m_{Added} [kg]
1-a	154.4	35.6	10.47	0	10.57	0	10.45	-
2-a	154.4	64.6	7.78	0	7.76	0	7.76	-
3-a	281.6	36.0	14.07	0	13.89	0	14.00	-
4-a	281.6	65.0	10.48	0	10.44	0	10.44	-
1-w	154.4	35.6	6.75	50.3	6.53	56.1	6.99	48.4
2-w	154.4	64.6	5.83	50.3	5.70	56.0	5.99	48.4
3-w	281.6	36.0	9.09	50.3	8.74	57.3	9.42	48.4
4-w	281.6	65.0	7.87	50.3	7.63	57.6	8.07	48.5
1-p	154.4	35.6	6.75	50.3	6.44	58.6	6.94	49.6
2-p	154.4	64.6	5.83	50.3	5.63	58.6	5.96	49.5
3-p	281.6	36.0	9.09	50.3	8.65	59.3	9.37	49.2
4-p	281.6	65.0	7.87	50.3	7.57	59.5	8.04	49.4

5.5 Discussion

A fundamental difference in the results from the experiments and the model is that the frequency differs. This has effects on the amplitude of the acceleration and the values of the pressure. When the acceleration from the model was adjusted to the frequency of the experiment the results are similar. A difference is the reduction in amplitude for the experimental values, this is due to decay in the wave which is not present in the model.

The measured pressure is different from the modelled and the results shows that the pressure behaves in a different way. It is believed that the sudden changes in pressure in the FE-model are due to acoustic waves transmitting pressure at a speed of $1500m/s$. These pressure waves are not captured properly in the fringe plots as the time step is too large.

From (5.1) it can be seen that there is a clear difference in added mass between the experiments and the models. What is interesting is that according to the analytical solution added mass should be constant between all the load cases. However the experiments capture an increase in added mass as the box becomes heavier and as the springs change from weak to strong. The increase in added mass from the change of springs does not necessarily follow as a result of an increased spring constant. Depending on what springs are used the distance between the box and the frame changes from $77mm$ for the weaker springs and $94mm$ for the stronger. It could also be due to more viscous effects that the stiffer springs introduce due to being larger. Unfortunately it can not be determined whether it is the distance to the plate, the spring constant or viscous effects that influences added mass.

As the plate is introduced added mass for both the experiments and the simulations changes slightly. The addition of the plate increases added mass in both the experiment and in the simulations. This shows that the model interprets the effect of the plate in the same way as in the experiments.

6 Conclusion

In fluid structure interaction, added mass is a central concept regarding movement of a structure in water. This report provides an assessment of modelling of added mass using the element formulation `Mat_Acoustic` in LS-DYNA. Experiments were conducted with an oscillating submerged box using different spring constants and mass. A model of the experiment was constructed and simulated in LS-DYNA. The results from the simulations were compared to the experimental data. It is shown that added mass is consistently underestimated by 15% in the FE-model. The used analytical solution and `Mat_Acoustic` provide similar lower estimates of the added mass. If the analytical assessment using a sphere was to be used instead of a cylinder the FE-model would outperform the analytic assessment as the spherical assessment provides an added mass more than 40% lower compared to the experiments. Keep in mind that for more complex geometries analytical solutions are not available. In those cases `Mat_Acoustic` can be used as it allows for an approximation of the added mass.

There are other ways to model fluid structure interaction in use by Kockums today. The main advantage of `Mat_Acoustic` is that it uses only one degree of freedom per fluid element node resulting in a computationally efficient model. This allows for computation of added mass for large and complex models which otherwise would have been too expensive. A change in the fluid structure interaction was introduced by the mounting of a plate beneath the box. The results from the addition of the plate were studied for both the experiment and the model. In the experiments the plate resulted in a $4 \pm 1\%$ increase of added mass. Whereas in the model the plate resulted in a $2 \pm 0.5\%$ increase of added mass. `Mat_acoustic` succeeds to represent tendencies of the fluid structure interaction as it was observed in the experiment.

Three convergence studies were performed. The required fluid size to validate the assumptions of infinite fluid volume was tested for an oscillating solid box. It was found that infinite fluid volume can be assumed when there is fluid in all directions a distance of 1.4 times a characteristic length.

A fluid element size study was also performed. This time for an oscillating shell structure. Here it was discovered that for certain element sizes the model was unstable as the structure deformed unexpectedly. The deformation could be avoided by increasing the stiffness of the structure. As the model becomes unstable an interference pattern in the fluid pressure was observed in the convergence study. It is not known whether the interference pattern causes the instability or is consequence of it. The frequency was found to decrease linearly with element size but full convergence was not reached. However, the frequency for ratios between the structure and the fluid elements under 0.025 were of similar value and determining a mesh size becomes a trade off between computational cost and required accuracy.

The same study was also performed for a solid box. Here it was found that the fluid elements should be kept smaller than 7% of the structure's characteristic length for the results to converge. The structure experienced no deformation or stability issues as a solid.

In the model, the coupling between the fluid and the structure does not change position as the structure moves. For small deformations this assumption holds however with large deformations `Mat_Acoustic` should be used with caution as the load on the structure is calculated as if no deformation has occurred. This explains why the modelling of shell elements is more unstable compared to solids as solids experience less deformation.

The damping in the experiments was measured and it was found that the decay can accurately be approximated by two exponential terms. The approximation shows that there are two damping phenomena in the experiment, one dominating in the beginning and one in the end. Constants for the decay approximation were generated for all experiments and are available for future use.

7 Recommendations for Use of Mat_Acoustic

In this thesis, experimental data was gathered and compared to simulations using Mat_Acoustic. Moreover, convergence studies for basic models were performed. The knowledge from the simulations combined with the acquired experience from trial and error resulted in the following set of recommendations for Mat_Acoustic.

- Symmetry can be used to speed up the FE-model without affecting the results.
- Density scaling can be used without affecting the added mass.
- Use Spc_Set to model rigid boundaries.
- Leave surfaces that should be modelled as infinite water or as water in contact with air untouched.
- For a solid structure the results converge at a mesh size of 0.075 times a characteristic length of the structure.
- For a shell structure small element sizes should be used to maintain stability in the FE-model. Convergence of results was never fully achieved. In terms of stability, fluid element sizes of less than 0.025 times a characteristic length are recommended.
- Modelling of fluid further away from the structure than 1.4 times a characteristic length of the structure has no effect on the results if the boundary is not rigid.
- Large displacements of the structure can be modelled however large deformation can cause instability. Increasing Young's modulus is an option to increase stability.
- Acoustic mismatch has been found to work well. To use the mismatch coupling, the fluid mesh needs to adjoin the structure. The only thing which needs to be controlled is that the normal of the structure segment set points towards the fluid. Difficulties have arisen when coupling a shell element to both sides due to fluid elements penetrating the shell element.

In general Mat_Acoustic is a fast model to approximate added mass for complex geometries where analytic solutions are not available. However the results should be used with caution as models can be unstable. Furthermore the results should be seen as an approximation, as the model has been found to underestimate the added mass by 15% in the analyzed case.

8 Future work

The effect of the plate was rather small and it would be interesting to investigate the fluid-structure interaction of the plate for a more drastic case. This would be beneficial as the fluid-structure interactions of the frame is believed to dominate in the current setup. What happens if the plate is moved closer to the box, how well will the FE-model then be able to capture the interaction?

For the investigated box geometry added mass is underestimated. Is this specific to the geometry or is this a reoccurring result? To investigate this further it is proposed that different geometries of the box should be tested. This would provide more general conclusions in Mat_Acoustics capabilities of calculating added mass.

Frequencies ranging from 5.6 to 8.7 Hz have been tested in water. A larger frequency span would allow for more definitive conclusions regarding the effects of frequency on added mass. How does the frequency affect damping? A model of decay has been proposed but more trials are required in order to determine its parameters. For use in design perhaps only a model of the initial damping would suffice.

In the convergence study with shell elements some models failed. The reason for failure is not determined although it is believed to be related to deformation of the structure. Failure was dependent of fluid mesh size however further investigation would increase the knowledge of stability of different meshes.

As the coupling between the fluid and the structure is fixed in space, errors are introduced with displacements of the structure. How does the displacements influence the results? It would be of interest to perform a convergence study of different amplitudes to investigate this source of error.

References

- [1] C.E. Brennen. *A review of added mass and inertial forces*. Last visited on 08/06/2017. 1982. URL: <http://authors.library.caltech.edu/233/1/BRE052.pdf>.
- [2] C.A. Felippa and J.A. Deruntz. “Finite Element Analysis of Shock-Induced Hull Cavitation”. In: *Computer Methods in Applied Mechanics and Engineering* 44 (1984), pp. 297–337.
- [3] P. Davidsson G. Sandberg P-A. Wernberg. “Fundamentals of Fluid-Structure Interaction”. In: (). Not published.
- [4] Jensen F.B.; Kuperman W.A.; Porter M.B.; Schmidt H. *Computational Ocean Acoustics*. Springer, 2011.
- [5] L. Hammond and R. Grzebieta. “The requirement for hydrostatic initialisation in LS-DYNA/USA finite element models”. In: *Shock and Vibration 7 (2000)* (1999), pp. 57–65.
- [6] J.-Ph. Ponthon J.Donea A. Huerta and A. Rodríguez-Ferran. *Encyclopedia of Computational Mechanics*. Wiley, 2004.
- [7] LSTC. *LS-DYNA Keyword User’s Manual Volume I*. Last visited on 08/06/2017. URL: http://lstc.com/pdf/ls-dyna_971_manual_k.pdf.
- [8] LSTC. *LS-DYNA Keyword User’s Manual Volume II Material Models*. Last visited on 09/06/2017. URL: http://ftp.lstc.com/anonymous/outgoing/jday/manuals/DRAFT_Vol_II.pdf.
- [9] LSTC. *LS-DYNA Theory Manual*. Last visited on 08/06/2017. URL: http://ftp.lstc.com/anonymous/outgoing/jday/manuals/DRAFT_Theory.pdf.
- [10] LSTC. *Shell Formulation*. Last visited on 08/06/2017. URL: <http://www.dynasupport.com/howtos/element/shell-formulations>.
- [11] LSTC. *Usage of the Displacement Potential Formulation in LS-DYNA*. 2016.
- [12] LSTC. *What are the differences between implicit and explicit*. Last visited on 08/06/2017. URL: <http://www.dynasupport.com/faq/general/what-are-the-differences-between-implicit-and-explicit>.
- [13] J. L. Meriam and L.G. Kraige. *Engineering Mechanics Dynamics*. John Wiley & Sons, Inc, 2013.
- [14] Lars Olovsson. *Training class in ALE and fluid-structure interaction*. Last visited on 08/06/2017. URL: ftp://ftp.lstc.com/outgoing/jday/ALE_training_by_Lars.Sept06.pdf.
- [15] A. V. Oppenheim. *Butterworth Filters*. Last visited on 08/06/2017. URL: https://ocw.mit.edu/resources/res-6-007-signals-and-systems-spring-2011/lecture-notes/MITRES_6_007S11_lec24.pdf.
- [16] N. S. Ottosen and H. Pettersen. *Introduction to the finite element method*. Harlow: Prentice Hall, 1992.

A Keywords

A.1 Box and Frame

The screenshot shows a software interface for defining material properties. At the top is a 'TITLE' field. Below it, a table of parameters is displayed for material ID 1. The parameters and their values are:

MID	RO	E	PR	DA	DB	NOT USED
1	7850.0000	2.100e+11	0.3000000	0.3000000	0.0	0

Figure A.1: A print screen of the different parameters for Mat_Elastic. RO is the density, E is the Young's Modulus and PR is Poisson's Ratio, all in SI-units. The density shown here was used for the frame whilst the density of the box was scaled to change its mass.

The screenshot shows a software interface for defining shell section properties. It features a 'TITLE' field and two rows of parameters for section ID 1 and 2. The parameters and their values are:

SECID	ELFORM	SHRF	NIP	PROPT	QR/IRID	ICOMP	SETYP
3	16	0.8333330	7	1	0	0	1
T1	T2	T3	T4	NLOC	MAREA	IDOF	EDGSET
0.0050000	0.0050000	0.0050000	0.0050000	0.0	0.0	0.0	0

Figure A.2: A print screen of the different parameters for the shell sections. Some things to keep in mind are that element formulation 16 is used, SHRF is set to the recommended value of 5/6 (not default) and 7 NIP are used. T1-T4 denotes the thickness which in this case is the thickness of the box.

A.2 Fluid Volume

The screenshot shows a software interface for defining acoustic material properties. It includes a 'TITLE' field and two rows of parameters for material ID 10. The parameters and their values are:

MID	RO	C	BETA	CF	ATMOS	GRAV
10	1000.00000	1480.0000	0.5000000	0.0	0.0	0.0
XP	YP	ZP	XN	YN	ZN	
0.0	0.0	0.0	0.0	0.0	0.0	

Figure A.3: A print screen of the different parameters for Mat_Acoustic. RO is the density, C is the speed of sound in water, and beta is a damping coefficient used to make the computations more stable and to reduce frothing.

The screenshot shows a software interface for defining section properties for a solid. It features a 'TITLE' field and a single row of parameters for section ID 10. The parameters and their values are:

SECID	ELFORM	AET
10	8	0

Figure A.4: A print screen of the different parameters for Section_Solid. Acoustic elements (ELFORM 8) are used for Mat_Acoustic.

A.3 Springs

TITLE

1 **SECID** **DRO** **KD** **VO** **CL** **FD**

50 0 0.0 0.0 0.0 0.0

2 **CDL** **TDL**

0.0 0.0

Figure A.5: Only default options were used.

TITLE

1 **MID** **K**

11 7.039e+04

Figure A.6: The spring constant could be adjusted depending on the springs.

A.4 Hourglassing and Control Keywords

TITLE

1 **HGID** **IHQ** **QM** **IBQ** **Q1** **Q2** **QB/DC** **QW**

51 8 0.1000000 0 1.5000000 0.0600000 0.1000000 0.1000000

Figure A.7: IHQ=8 is often used together with element formulation 16.

1 **OSU** **INN** **PIDOSU** **IACC**

0 2 0 0

Figure A.8: INN=2 is recommended in the Control_Accuracy keyword

1 **Q1** **Q2** **TYPE** **BTYPE**

1.5000000 0.0600000 -1 0

Figure A.9: Note that TYPE=-1 is not a default value

1 **HGEN** **RWEN** **SLNTEN** **RYLEN**

2 2 2 2

Figure A.10: The following settings includes all energies in the energy balance and was used.

B Measuring devices

Information about the used measuring devices are presented in the table below.

Table B.1: Used measuring devices

Device	Type	Serial	Additional device	Type	Serial
Position Sensor 1	ACW200013/7	3636	Power Supply	S7AC	33001
Position Sensor 2	ACW200013/7	3641	Power Supply	S7AC	33002
Position Sensor 3	ACW200013/7	3637	Power Supply	S7AC	32329
Accelerometer Top	4382	2227392	Charge Amplifier	2635	2002863
Accelerometer Bottom	4382	2227395	Charge Amplifier	2635	2002864
Pressure Top	-	47012	Charge Amplifier	2635	2002862
Pressure Bottom	-	48050	Charge Amplifier	2635	1575692
Strain Gauge	-	-	-	-	-